

# Probes of Lorentz Violation in Neutrino Propagation

John Ellis<sup>1</sup>, Nicholas Harries<sup>1,2</sup>, Anselmo Meregaglia<sup>3</sup>, André Rubbia<sup>4</sup> and  
Alexander S. Sakharov<sup>1,4</sup>

<sup>1</sup> *TH Division, PH Department, CERN, CH-1211 Geneva 23, Switzerland*

<sup>2</sup> *Theoretical Physics, University of Oxford, 1Keble Road, Oxford, UK*

<sup>3</sup> *IPHC, Universit , Louis Pasteur, CNRS/IN2P3, Strasbourg, France*

<sup>4</sup> *Swiss Institute of Technology ETH-Z rich, CH-8093 Z rich, Switzerland*

## Abstract

It has been suggested that the interactions of energetic particles with the foamy structure of space-time thought to be generated by quantum-gravitational (QG) effects might violate Lorentz invariance, so that they do not propagate at a universal speed of light. We consider the limits that may be set on a linear or quadratic violation of Lorentz invariance in the propagation of energetic neutrinos,  $v/c = [1 \pm (E/M_{\nu QG1})]$  or  $[1 \pm (E/M_{\nu QG2})^2]$ , using data from supernova explosions and the OPERA long-baseline neutrino experiment. Using the SN1987a neutrino data from the Kamioka II, IMB and Baksan experiments, we set the limits  $M_{\nu QG1} > 2.7(2.5) \times 10^{10}$  GeV for subluminal (superluminal) propagation, respectively, and  $M_{\nu QG2} > 4.6(4.1) \times 10^4$  GeV at the 95 % confidence level. A future galactic supernova at a distance of 10 kpc would have sensitivity to  $M_{\nu QG1} > 2(4) \times 10^{11}$  GeV for subluminal (superluminal) propagation, respectively, and  $M_{\nu QG2} > 2(4) \times 10^5$  GeV. With the current CNGS extraction spill length of  $10.5 \mu\text{s}$  and with standard clock synchronization techniques, the sensitivity of the OPERA experiment would reach  $M_{\nu QG1} \sim 7 \times 10^5$  GeV ( $M_{\nu QG2} \sim 8 \times 10^3$  GeV) after 5 years of nominal running. If the time structure of the SPS RF bunches within the extracted CNGS spills could be exploited, these figures would be significantly improved to  $M_{\nu QG1} \sim 5 \times 10^7$  GeV ( $M_{\nu QG2} \sim 4 \times 10^4$  GeV). These results can be improved further if similar time resolution can be achieved with neutrino events occurring in the rock upstream of the OPERA detector: we find potential sensitivities to  $M_{\nu QG1} \sim 4 \times 10^8$  GeV and  $M_{\nu QG2} \sim 7 \times 10^5$  GeV.

CERN-PH-TH/2008-088

April 2008

# 1 Introduction

Neutrinos from astrophysical sources and long-baseline experiments are powerful probes of potential new physics. They have already been used to discover and measure the novel phenomena of neutrino oscillations, thereby establishing that neutrinos have masses [1, 2]. Long-baseline neutrino experiments have also been used to set limits on quantum decoherence effects that might be induced by foamy fluctuations in the space-time background in some models of quantum gravity (QG) [3–6]. It has also been suggested that the space-time foam due to QG fluctuations might cause energetic particles to propagate at speeds different from the velocity of light, which would be approached only by low-energy massless particles [7, 8]. Any deviation from the velocity of light at high energies might be either linear or quadratic,  $\delta v/c = (E/M_{QG1})$  or  $(E/M_{QG2})^2$ , and might be either subluminal or superluminal. Such effects are, in principle, easily distinguishable from the effects of neutrino masses, since they depend differently on the energy  $E$ .

There have been many tests of such Lorentz-violating effects on photon propagation from distant astrophysical objects such as gamma-ray bursts [9], pulsars [10] and active galactic nuclei [11]. These tests have looked for delays in the arrival times of energetic photons relative to low-energy photons, and their sensitivities improve with the distance of the source, the energies of the photons, the accuracy with which the arrival times of photons can be measured, and the fineness of the time structure of emissions at the astrophysical source. The sensitivities of these tests has reached  $M_{\gamma QG1} \sim 2 \times 10^{17}$  GeV and  $M_{\gamma QG2} \sim 4 \times 10^{10}$  GeV for linear and quadratic violations of Lorentz invariance, respectively.

At least one QG model of space-time foam [12, 13] suggests that Lorentz violation should be present only for particles without conserved internal quantum numbers, such as photons, and should be absent for particles with electric charges, such as electrons. Indeed, astrophysical data have been used to set very stringent limits on any Lorentz violation in electron propagation. However, these arguments do not apply to neutrinos, since they are known to oscillate, implying that lepton flavour quantum numbers are not conserved. Moreover, neutrinos are often thought to be Majorana particles, implying that the overall lepton number is also not conserved, in which case QG effects might also be present in neutrino propagation [14]. It therefore becomes interesting to study experimentally the possibility of Lorentz violation in neutrino propagation.

Experimental probes of Lorentz violation in neutrino propagation are hindered by the relative paucity of neutrino data from distant astrophysical sources, and require the observation of narrow time structures in neutrino emissions. However, there has been one pioneering experimental study of possible Lorentz violation using the long-baseline MINOS experiment exposed to the NuMI neutrino beam from Fermilab, which found a range of neutrino velocities  $-2.4 \times 10^{-5} < (v - c)/c < 12.6 \times 10^{-5}$  allowed at the 99% C.L. [15]. Assuming an average neutrino energy of 3 GeV, and allowing for either linear or quadratic Lorentz violation:  $v/c = [1 \pm (E/M_{\nu QG1})]$  or  $[1 \pm (E/M_{\nu QG2})^2]$ , the MINOS result [15] corresponds in the case of linear Lorentz violation to  $M_{\nu QG1} > 1(4) \times 10^5$  GeV in the case of subluminal (superluminal) propagation, and in the case of quadratic Lorentz violation to  $M_{\nu QG2} > 600(250)$  GeV.

In this paper we first establish limits on Lorentz violation using neutrino data from supernova 1987a, using data from the Kamioka II (KII) [16], Irvine-Michigan-Brookhaven (IMB) [17] and Baksan detectors [18]. We find  $M_{\nu_{QG1}} > 2.7(2.5) \times 10^{10}$  GeV for subluminal (superluminal) propagation, respectively, and  $M_{\nu_{QG2}} > 4.6(4.1) \times 10^4$  GeV at the 95 % confidence level. These limits are already much more stringent than those established using the MINOS detector. We then assess the improved sensitivity to Lorentz violation that could be obtained if a galactic supernova at a distance of 10 kpc is observed using the Super-Kamiokande detector, estimating sensitivities to  $M_{\nu_{QG1}} > 2(4) \times 10^{11}$  GeV for subluminal (superluminal) propagation, respectively, and  $M_{\nu_{QG2}} > 2(4) \times 10^5$  GeV. All these results are obtained taking neutrino oscillation effects into account, and assuming that any Lorentz violation is flavour-independent <sup>1</sup>.

We also discuss the sensitivity to Lorentz violation of the OPERA experiment at the CNGS neutrino beam from CERN <sup>2</sup>. We recall that the CNGS beam cycle provides two fast-extracted proton spills lasting 10.5  $\mu$ s each and separated by 50 ms, each containing 2100 bunches with standard deviation 0.25 ns, separated from each other by the CERN SPS RF bucket structure of 5 ns [20]. The OPERA data-acquisition (DAQ) system is organized in such a way that each subdetector provides its data with a distributed time-stamp with a granularity of 10 ns. If a time-synchronization method conceptually similar to that of MINOS between the CERN neutrino extraction-magnet signal and the OPERA time-stamp were implemented, the sensitivity would be greater than that of MINOS. This because, even though the baseline between the source and the detector are the same and the spill lengths are similar, the neutrinos in the CNGS beam typically have higher energies than those in the NuMI beam. Exploiting this feature, on the basis of an optimized analysis we estimate that after 5 years of running sensitivities using OPERA could reach  $M_{\nu_{QG1}} \sim 7 \times 10^5$  GeV ( $M_{\nu_{QG2}} \sim 8 \times 10^3$  GeV) for subluminal (superluminal) propagation.

Further improvements in sensitivity would result if one could exploit the RF bucket structure of the spill. Assuming that the arrival time of the neutrinos would be correlated with the RF bunch structure with a timing accuracy of, say, 1 ns, the sensitivity to Lorentz violation could be improved to  $M_{\nu_{QG1}} \sim 5 \times 10^7$  GeV ( $M_{\nu_{QG2}} \sim 4 \times 10^4$  GeV) for the linear and quadratic cases, respectively. These results could be improved significantly if neutrino events occurring in the rock upstream from OPERA could be included in the analysis. In this case, the sensitivities would become  $M_{\nu_{QG1}} \sim 4 \times 10^8$  GeV and  $M_{\nu_{QG2}} \sim 7 \times 10^5$  GeV. In the case of quadratic Lorentz violation, this sensitivity is better than that obtained from supernova 1987a, and even improves on the sensitivity possible with a future galactic supernova.

---

<sup>1</sup>This is a strong condition on any model of Lorentz violation, that is imposed by the success of conventional neutrino oscillation phenomenology, which implies that flavour-dependent dispersion effects can be neglected in the analyses of MINOS and OPERA data. Such effects could in principle appear in neutrinos from supernovae, but would not affect the results presented below, which are essentially independent of oscillation hypotheses.

<sup>2</sup>For previous discussions of searches for Lorentz violation in neutrino data, see [14, 19].

## 2 Limits on Lorentz Violation from Supernovae

In this Section we discuss the supernova mechanism and the ability to test Lorentz violation via the detection of neutrinos created in this process. We then analyze the data from the supernova SN1987a, the first supernova from which neutrinos have been detected, giving bounds at the 95% C.L.. Then we simulate a possible future galactic supernova and discuss the potential of the next generation of neutrino detectors, represented by Super-Kamiokande (SK), to improve this bound.

### 2.1 Review of Neutrino Emissions from Supernovae

The detection of neutrinos from SN1987a in the Large Magellanic Cloud (LMC) remains a landmark in neutrino physics and astrophysics. Although only a handful of neutrinos were detected by the Kamiokande-II (KII) [16], Irvine-Michigan-Brookhaven (IMB) [17] and Baksan [18] detectors, they provided direct evidence of the mechanism by which a star collapses, and the role played by neutrinos in this mechanism [2]. The numbers and energies of the neutrinos observed were consistent with the expected supernova energy release of a few times  $10^{53}$  ergs via neutrinos with typical energies of tens of MeV. A future galactic supernova is expected to generate up to tens of thousands of events in a water-Čerenkov detector such as SK, which will clarify further theories of the supernova mechanism and of particle physics [21].

Current simulations reveal several distinct stages of neutrino emission [22–24]. During the early stage with a typical timescale of a few milliseconds, huge numbers of  $\nu_e$  are produced via  $pe \rightarrow n\nu_e$ , known as the neutronization peak. Despite the huge numbers of neutrinos produced, these are difficult to detect with water-Čerenkov detectors, because the neutrinos produced in this process are detected via scattering on electrons and (in the case of the electron neutrino) via interactions with Oxygen nuclei. At the energies of interest the cross section for detection is dominated by the charged-current interaction  $\bar{\nu}_e p \rightarrow n e^+$ , which detects anti-electron neutrinos. During the later stages of the supernova explosion, all flavours of neutrinos and antineutrinos are produced with approximate Fermi-Dirac spectra, that are characterized by different average energies for different neutrino species:  $\langle E_{\nu_e} \rangle = (10 - 12)$  MeV,  $\langle E_{\bar{\nu}_e} \rangle = (12 - 18)$  MeV and  $\langle E_{\nu_x} \rangle = (15 - 28)$  MeV (where  $\nu_x$  denotes  $\nu_\mu, \nu_\tau$  and their respective antiparticles), with total emitted energy fractions  $\varepsilon_{\nu_e} = (10 - 30)\%$ ,  $\varepsilon_{\bar{\nu}_e} = (10 - 30)\%$ ,  $\varepsilon_{\nu_x} = (10 - 20)\%$  [23, 24].

The neutrinos produced in the supernova pass from densities close to nuclear density in the core through to the approximate vacuum of interstellar space, and the interactions with this matter dominate the neutrino oscillations. The neutrinos become maximally mixed at Mikheev-Smirnov-Wolfenstein (MSW) resonances and to first approximation the nature of the oscillations can be determined by the properties of these resonances. The resonance condition is  $A = \Delta m^2 \cos 2\theta$ , where  $A$  is the matter potential,  $\Delta m^2$  is the difference in mass squared and  $\theta$  is the mixing angle. For a typical density profile and composition of the supernova medium, and typical neutrino energies, the matter potential is positive (negative) for neutrinos (antineutrinos). Assuming just the three Standard Model neutrinos, there are

Hierarchy	$\sin^2 \theta_{13}$	p		$\bar{p}$
		$E < E_c$	$E > E_c$	
Normal	$\gtrsim 10^{-3}$	0	0	$\cos^2 \theta_\odot$
Inverted	$\gtrsim 10^{-3}$	$\sin^2 \theta_\odot$	$\sin^2 \theta_\odot$	0
Normal or Inverted	$\lesssim 10^{-5}$	$\sin^2 \theta_\odot$	$\sin^2 \theta_\odot$	$\cos^2 \theta_\odot$
Inverted SS	$\gtrsim 10^{-3}$	$\sin^2 \theta_\odot$	$\cos^2 \theta_\odot$	1
Inverted SS	$\lesssim 10^{-5}$	$\sin^2 \theta_\odot$	$\cos^2 \theta_\odot$	$\sin^2 \theta_\odot$

Table 1: *The oscillation probabilities for the normal and inverse hierarchies, including the effect of the spectral split (SS), where the resulting  $\nu_e$  and  $\bar{\nu}_e$  fluxes are  $F_{\nu_e} = pF_{\nu_e}^0 + (1-p)F_{\nu_x}^0$  and  $F_{\bar{\nu}_e} = \bar{p}F_{\bar{\nu}_e}^0 + (1-\bar{p})F_{\bar{\nu}_x}^0$  respectively.*

two possible MSW resonances, corresponding to the solar and atmospheric mass-squared splittings [25–27]. We know from the solar and KamLAND data that  $\Delta m_{21}^2 \equiv m_2^2 - m_1^2$  is positive, and therefore the corresponding MSW resonance is in the neutrino sector [28].

However, the sign of  $\Delta m_{32}^2$  is undetermined and therefore the corresponding resonance could be in either the neutrino or the antineutrino sector, corresponding to the two possible mass hierarchies, the normal (inverted) for a positive (negative)  $\Delta m_{32}^2$ . At the resonance there is a probability of transitions between the mass eigenstates, known as ‘level crossing’. If the width of the resonance is large compared to the neutrino oscillation length at the resonance then the level crossing probability is small and the resonance is adiabatic. On the other hand, if the width of the resonance is small compared to the neutrino oscillation length scale, then transitions between the mass eigenstates occur and the resonance is said to be non-adiabatic. Combining current simulations of the supernova and the value of the solar mixing angle we can determine that the solar resonance is adiabatic [1]. However, the current limit on  $\theta_{13}$  is insufficient to determine whether the atmospheric resonance is adiabatic or not: simulations indicate that if  $\sin^2 2\theta_{13} \gtrsim 10^{-3}$  the resonance is adiabatic and if  $\sin^2 2\theta_{13} \lesssim 10^{-5}$  the resonance is non-adiabatic. The oscillation probabilities for both hierarchies are given in Table 1.

In addition to these effects, recent work has shown that neutrino self-interactions can induce large, non-MSW flavour oscillations [29]. These occur at large neutrino densities, just outside the neutrinosphere. For the normal hierarchy these effects have little effect on the flavour oscillations, but for the inverted hierarchy with non-zero  $\theta_{13}$  significant flavour changes can occur. These effects result in a ‘spectral split’, in which the  $\nu_e$  and  $\nu_x$  spectra are simply swapped above a critical energy, while the entire spectra of the  $\bar{\nu}_e$  and  $\bar{\nu}_x$  are swapped. For the case where the flavour transformations have occurred before the MSW resonances the flavour transformations can be thought of as changing the initial spectra, whereas in the case of shallow density profiles this becomes more complicated.

We note in addition that, as the shock wave inside the supernova passes through the atmospheric resonance, it can change it from adiabatic to non-adiabatic, resulting in a time dependence in the signal that we do not consider in this paper [30].

## 2.2 Analysis Techniques

As previously discussed, it has been suggested that QG effects may lead to Lorentz-violating modifications in the propagation of energetic particles, and hence to dispersive effects, specifically a non-trivial refractive index. These dispersive properties of the vacuum would lead to an energy dependence in the arrival times of neutrinos.

Even in the absence of any detailed, analytic understanding of time structure of a neutrino signal from a supernova, one can exploit the observation that, since the neutrino events have a range of energies, an energy dependence of the neutrino velocity would spread out the arrival times, compared to the signal if there were no dispersive properties of the vacuum. Any data set comprising both the time and energy of each neutrino event can be analyzed by inverting the dispersion that would be caused by any hypothesized QG effect. The preferred value of the energy-dependence parameter would minimize the duration (time spread) of the supernova neutrino signal.

Assuming either a linear or a quadratic form of Lorentz violation:  $v/c = [1 \pm (E/M_{\nu QG1})]$  or  $[1 \pm (E/M_{\nu QG2})^2]$ , a lower limit on  $M_{\nu QG1}$  and  $M_{\nu QG2}$  may be obtained by requiring that the emission peak not be broadened significantly. A non-zero value of  $M_{\nu QG1}^{-1}$  or  $M_{\nu QG2}^{-1}$  might be indicated if it reduced significantly the duration (time spread) of the neutrino signal. The duration (time spread) of the neutrino signal can be quantified using different estimators depending mostly on the amount of available statistics and time profile of the data set, if applicable<sup>3</sup>. In the following, we outline two estimators for analyzing neutrino signals, that we use first to quantify the limits obtainable from the SN1987a neutrino data and then the sensitivities that would be provided by a possible future galactic supernova signal.

### 2.2.1 Minimal Dispersion (MD) Method

We assume that the data set consists of a list of neutrino events with measured energies  $E$  and arrival times  $t$  such as that in Table 2. In the first method, we consider event lists with a relatively low number of events, that do not allow a reasonable time profile to be extracted. In this case we consider the time dispersion of the data set, quantified by

$$\sigma_t^2 \equiv \langle (t - \langle t \rangle)^2 \rangle, \quad (1)$$

where  $t$  is the time of each detected event. We then apply an energy-dependent time shift  $\Delta t = \tau_l E^l$ , where  $\tau_l = L/cM_{\nu QGl}^l$ , varying  $M_{\nu QGl}$  so as to remove any assumed dispersive effects.

The ‘correct’ value of the time shift  $\tau_l$  should always compress the arrival times of the neutrino events. Any other (‘incorrect’) value of  $\tau_l$  would spread in time the events relative to the ‘correct’ shift. Therefore, the dispersion (1) can be considered as an estimator to measure the degree of ‘compression’ of the neutrino events in time. In the following, we first apply this MD method in a warm-up exercise to the data from SN 1987a, and later we exhibit in subsection 2.4 the typical behaviour of this estimator versus  $\tau_l$  for hypothetical data from a possible future galactic supernova.

---

<sup>3</sup> Statistically poor event lists, such as that for SN1987a, the only one currently available in supernova neutrino astronomy, do not allow the time profile to be classified, because time binning is impractical and one cannot apply nonparametric statistical tests to unbinned data.

Evaluating the dispersion (1) one obtains

$$\sigma_t^2 = \langle (t - \tau_l E^l - \langle t - \tau_l E^l \rangle)^2 \rangle \quad (2)$$

$$= \langle t^2 \rangle - \langle t \rangle^2 - 2\tau_l (\langle t E^l \rangle - \langle t \rangle \langle E^l \rangle) + \tau_l^2 (\langle E^{2l} \rangle - \langle E^l \rangle^2). \quad (3)$$

Therefore, the dispersion of the ‘de-refracted’ time distribution is minimized by the parameter  $\tau_l^{min}$ , defined by

$$\tau_l^{min} \equiv \frac{\langle t E^l \rangle - \langle t \rangle \langle E^l \rangle}{\langle E^{2l} \rangle - \langle E^l \rangle^2}. \quad (4)$$

We can use (4) for any data set to estimate the scale  $M_{\nu QGl}$  at which Lorentz violation is manifest. However, there are uncertainties in the energy and time measurements, as well as statistical uncertainties in the estimation of the observables calculated from any given data set, compared to their true values. We estimate the statistical uncertainties of an observable  $x$  as

$$\sigma_x^{stat} = \sqrt{\frac{\langle x^2 \rangle - \langle x \rangle^2}{N}}, \quad (5)$$

where  $N$  is the number of events, and  $x = E, t$  or some combination of both. In order to estimate the uncertainties in  $\tau_l^{min}$ , we use a Monte Carlo simulation to repeat the calculation of  $\tau_l^{min}$  including the energy and statistical uncertainties. We then make a Gaussian fit and use it to quote best-fit parameters and errors.

### 2.2.2 Energy Cost Function (ECF) Method

This is a different analysis technique that is mostly applicable to event lists that are statistically rich. This means that one can combine the neutrino events into a time profile exhibiting pulse features that can be distinguished (parametrically or nonparametrically) from a uniform distribution at high confidence level.

For the analysis we first choose the most active (transient) part of the signal ( $t_1; t_2$ ), as defined using a Kolmogorov-Smirnov (KS) statistic. The KS statistic is calculated using the difference between the cumulative distribution function (CDF) of the unbinned data and that of a uniform distribution. The KS statistic is defined as the time that elapses between the minimum and maximum of this difference<sup>4</sup>. Having chosen this window, we scan over its whole support the time distribution of all events, shifted by  $\Delta t = \tau_l E^l$ , and sum the energies of events in the window. This procedure is repeated for many values of  $\tau_l$ , chosen so that the shifts  $\Delta t$  match the precision of the arrival-time measurements, thus defining the ‘energy cost function’ (ECF). The maximum of the ECF indicates the value of  $\tau_l$  that best recovers the signal, in the sense of maximizing its power (amount of energy in a window of a given time width  $t_2 - t_1$ ). This procedure is then repeated for many Monte-Carlo (MC) data samples generated by applying to the measured neutrino energies the estimated Gaussian errors. A typical ECF for one particular MC realization as well as the typical distribution

---

<sup>4</sup> The most active part of the signal can be also chosen by fitting the binned time profile, but the non-parametric way we use to extract a feature is less dependent on the time profile. In the case of a multipulse structure of the time profile, several windows may be analyzed separately.

of the positions of the maxima of the ECFs for many energy MC realizations are illustrated in subsection 2.4 (see Fig. 5 and Fig. 6).

We perform this procedure for different energy weightings  $E^n$ , where  $n=0,1,2$ , summing up either the numbers of events, the energies or the squares of the energies in the time window selected, so to optimize the errors placed on the scale of Lorentz violation.

## 2.3 Data Analysis

For the analysis of SN1987a we use the uncertainties in Table 2, which were taken from [31]. In the case of a possible galactic supernova, we consider the Super-Kamiokande (SK) water Cerenkov detector, and we use the detector properties given in [30, 32], where the energy uncertainties are modelled as  $\sigma_E^{det2} = \sqrt{E_0 E}$ , where  $E_0 = 0.22$  MeV. We note that the uncertainties in the time measurements are in general much less than the statistical and energy uncertainties, and we therefore neglect them in our analysis.

IMB			Kamiokande II		
t (s)	E (MeV)	$\sigma_E$ (MeV)	t (s)	E (MeV)	$\sigma_E$ (MeV)
$t \equiv 0.0$	38	7	$t \equiv 0.0$	20.0	2.9
0.412	37	7	0.107	13.5	3.2
0.650	28	6	0.303	7.5	2.0
1.141	39	7	0.324	9.2	2.7
1.562	36	9	0.507	12.8	2.9
2.684	36	6	1.541	35.4	8.0
5.010	19	5	1.728	21.0	4.2
5.582	22	5	1.915	19.8	3.2
Baksan			9.219	8.6	2.7
t (s)	E (MeV)	$\sigma_E$ (MeV)	10.433	13.0	2.6
$t \equiv 0.0$	12.0	2.4	12.439	8.9	1.9
0.435	17.9	3.6			
1.710	23.5	4.7			
7.687	17.6	3.5			
9.099	10.3	4.1			

Table 2: *The measured neutrino data from SN1987a, where we have omitted the events identified previously as background, and in each data set we define  $t \equiv 0.0s$  for the first event.*

### 2.3.1 SN1987a

Neutrinos from SN1987a were detected in three detectors, KII, IMB and Baksan. The times and energies of the events are given in Table 2. The minimum dispersion was calculated 1000 times for each data set to include the smearing from uncertainties. As an example,



Fig. 1 shows this smearing for the KII data set. From these distributions we can determine the best fit and the error, which are summarized in Table 3. We analyze similarly the data from IMB and Baksan. As there is an uncertainty in the relative time measurements of each detector, we analyze each data set independently using the minimal dispersion method and then combine them to quote the final best fit and error, as shown in Table 3.

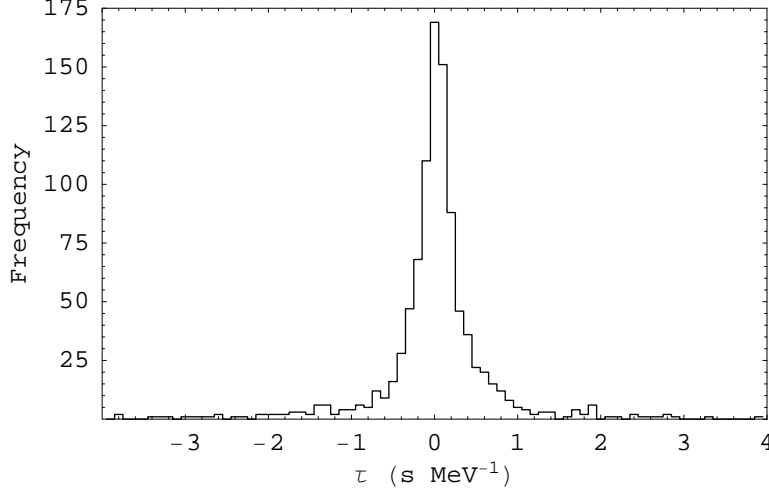


Figure 1: *The distribution  $\tau_{min}$  of 1000 Monte Carlo simulations of the KII data on neutrinos from SN1987a, including the smearing due to energy uncertainties.*

Data set	$\tau_1(\text{s} \cdot \text{MeV}^{-1})$		$\tau_2(10^{-3}\text{s} \cdot \text{MeV}^{-2})$	
	Best fit	Error	Best fit	Error
Kamiokande II	-0.0233307	0.197601	-0.685	2.935
IMB	-0.00417622	0.121513	-0.308	1.601
Baksan	0.0574167	0.47789	2.704	8.105
Combined	-0.00643648	0.101162	-0.304	1.385

Table 3: *The best fits to the SN1987a neutrino data obtained using the minimal dispersion method.*

On the basis of this combined analysis, Fig. 2 shows the region which is excluded by the SN1987a data. Taking the distance to the supernova as  $L = (51.3 \pm 1.2)$  kpc, the scale at which Lorentz violation may enter the neutrino sector is constrained to be

$$M_{\nu QG1} > 2.7 \times 10^{10} \text{ GeV} \text{ or } M_{\nu QG1} > 2.5 \times 10^{10} \text{ GeV} \quad (6)$$

at the 95% C.L. for the linear subluminal and superluminal models respectively. The corresponding limits for the quadratic models are

$$M_{\nu QG2} > 4.6 \times 10^4 \text{ GeV} \text{ or } M_{\nu QG2} > 4.1 \times 10^4 \text{ GeV} \quad (7)$$

at the 95% C.L. for the subluminal and superluminal versions, respectively.

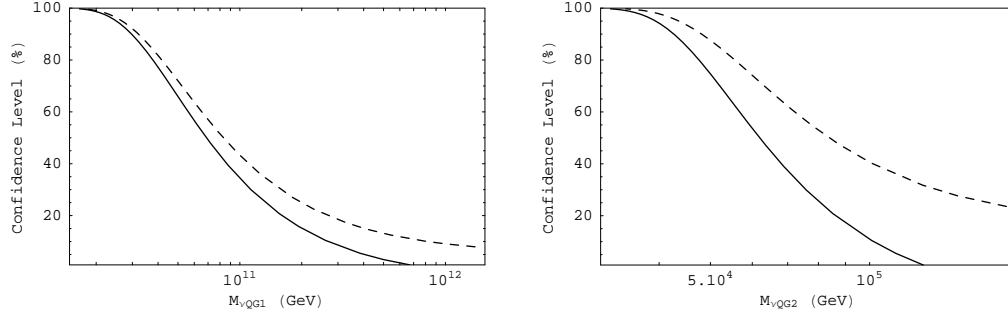


Figure 2: *The regions of parameter space excluded by SN1987a, for subluminal (dashing) and superluminal (black) linear (left) and quadratic (right) models.*

## 2.4 A Possible Future Galactic Supernova

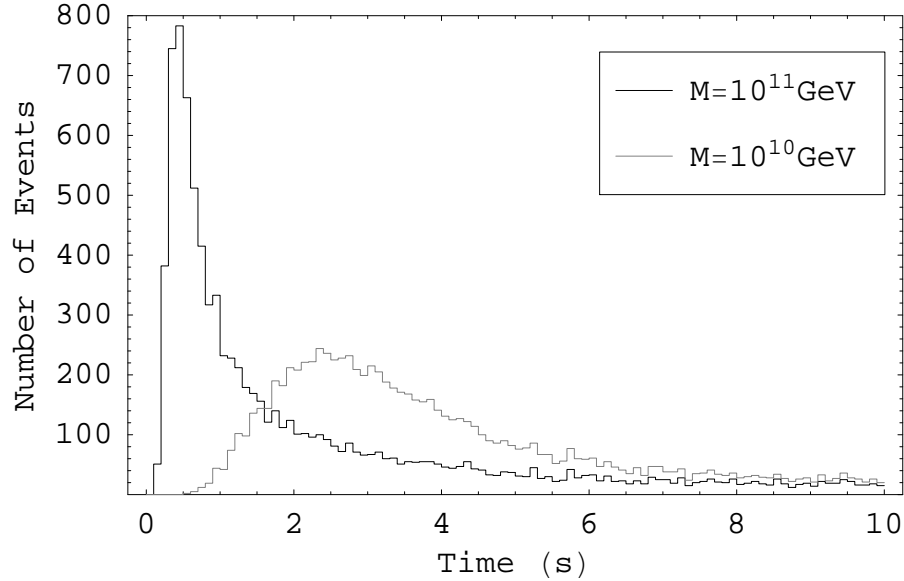


Figure 3: *The time distribution of events predicted by our Monte Carlo simulation for the case of subluminal Lorentz violation at the mass scales  $M = 10^{10}\text{GeV}$  and  $M = 10^{11}\text{GeV}$ .*

The detection of a galactic supernova would provide improved sensitivity to the scale at which Lorentz violation might enter the neutrino sector, due to an increase in the number of neutrinos which would be detected. The number of events would also increase because the current neutrino detectors are larger than those used to detect neutrinos from SN1987a. However, these effects would be partially offset because  $\tau_l \propto L$  and therefore the time-energy shift will be reduced if, as expected, the supernova takes place within the galactic disc at a distance  $\sim 10$  kpc, compared to SN1987a in the LMC at a distance of  $\sim 51$  kpc. The increase in the number of neutrinos which are expected to be detected are also because the next supernova is expected to be closer to the earth than SN1987a. For definiteness, we use

here a Monte Carlo simulation of the Super-Kamiokande (SK) neutrino detector, but note that other neutrino detectors could also probe this physics [33]. Simulations estimate that the number of events detected in SK from a supernova at 10 kpc would be of the order of 10,000 [21]. In order to analyze at what scales Lorentz violation could be probed by the detection of galactic supernova neutrinos, we made Monte Carlo simulations with various levels of linear and quadratic Lorentz violation. We used the energy spectra of neutrinos from the Livermore simulation [22], which is shown in Figure 4 and the detector properties given in [32].

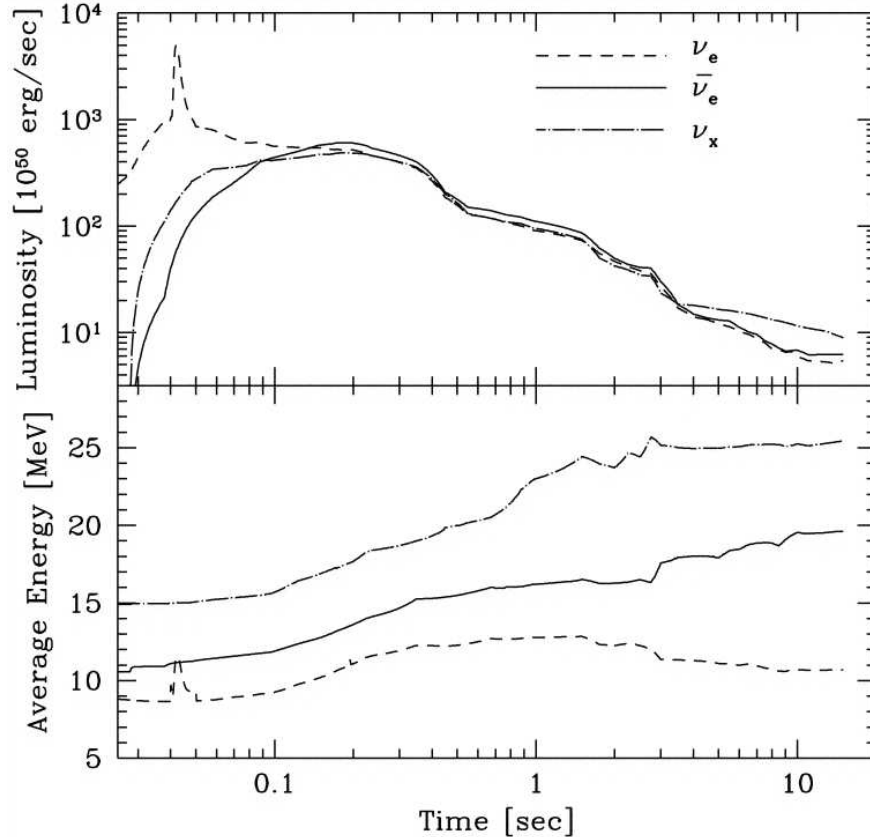


Figure 4: *The neutrino energy spectra from the Livermore simulation [22].*

We show in Fig. 3 results from our Monte Carlo simulation including both charged-current and neutral-current events for linear subluminal Lorentz violation at the energy scales  $M_{\nu QG1} = 10^{10} \text{ GeV}$  and  $M_{\nu QG1} = 10^{11} \text{ GeV}$ , including oscillations corresponding to the normal hierarchy and assuming that the atmospheric resonance is adiabatic. The signal has spread out and shifted in time, as we would expect. This time shift is unobservable because it is shifted relative to the signal in the absence of Lorentz violation, which in practice cannot be measured. We have applied the MD and the maximal ECF methods with various energy weightings to the Monte Carlo data with  $M_{QG1} = 10^{10} \text{ GeV}$  in order to estimate the level of Lorentz violation.

Fig. 5 shows the ECF for one realization of the energy-smeared sample obtained applying MC to the measured neutrino energies with the Gaussian errors expected from SK. It exhibits a clear maximum, whose position may be estimated by fitting it with a Gaussian profile in the peak vicinity. Fig. 6 shows the results of such fits to the ECFs constructed for the 1000 energy-smeared realizations. From this distribution we can derive the preferred value of  $\tau_l$ .

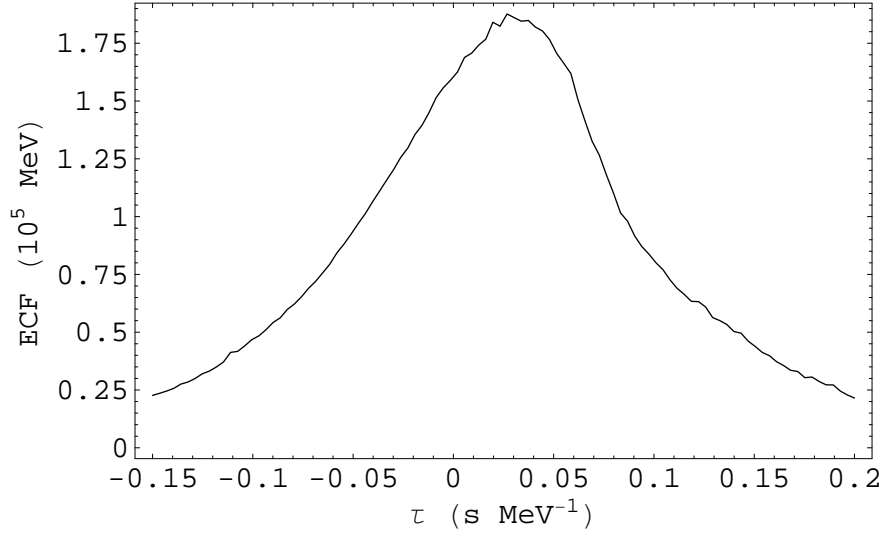


Figure 5: *The ECF linearly weighted with energy from one realization of the simulated time profile Fig. 3 with neutrino energies smeared by MC applying to the expected energy resolution of SK, for the case of linear energy depending neutrino velocity.*

The results are summarized in Table 4, where we have defined  $\hat{m}_l \equiv M_{\nu QGl}/M_{\nu QGl}^{true}$ , where  $M_{\nu QGl}^{true}$  is the true scale of Lorentz violation and  $M_{\nu QGl}$  is that deduced from the analysis method. Comparing these results, we find that the maximal ECF technique has greater sensitivity than the MD method, and that the linear energy weighting has the greatest sensitivity among the ECF analyses. We therefore use this in the following.

We have performed simulations for both the normal and inverted mass hierarchies, with and without the spectral splits caused by neutrino self-interactions, for the extreme cases  $P_H = 0.0$  and  $P_H = 1.0$ , and analysed them using the ECF method. The corresponding results are summarized in Table 5, where we see that Lorentz violation can be probed with similar sensitivity for all mass hierarchies.

The top three rows of Table 6 show the results of our analysis for the linear cases  $M_{\nu QG1} = (10^{10}, 10^{11}, 10^{12})$  GeV, using the minimal ECF method with no energy weighting, and making linear and quadratic fits. We see that data from a future galactic supernova could place strong 95% C.L. limits on the range of  $M_{\nu QG1}$  if it is lower than  $10^{11}$  GeV. In the limit of negligible Lorentz violation ( $M_{\nu QG1} \geq 10^{12}$  GeV), we find the lower limits  $M_{\nu QG1} > 2.2 \times 10^{11} \text{ GeV}$  and  $M_{\nu QG1} > 4.2 \times 10^{11} \text{ GeV}$  at the 95% C.L. for subluminal and superluminal models, respectively. The bottom three rows of Table 6 show the corresponding results for the quadratic cases  $M_{\nu QG2} = (10^{4.5}, 10^5, 10^{5.5})$  GeV, again using the minimal ECF method with

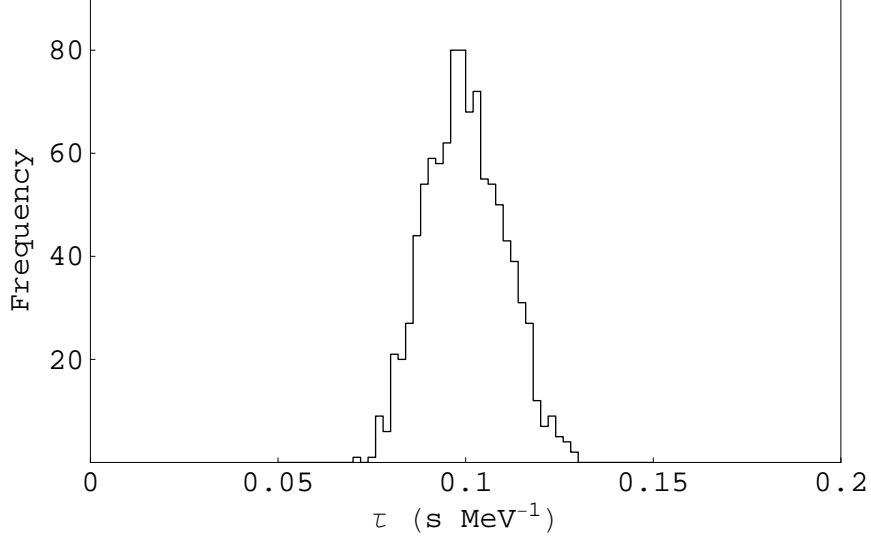


Figure 6: *The distribution of the positions of the maximums from fits of ECFs like in Fig. 5 of 1000 realizations of the simulated time profile Fig. 3 with neutrino energy smeared by MC.*

Method	95% C.L.
Minimal Dispersion (MD)	$0.60 < \hat{m}_1 < 2.37$
ECF 0th order	$0.90 < \hat{m}_1 < 1.29$
ECF 1st order	$0.88 < \hat{m}_1 < 1.26$
ECF 2nd order	$0.87 < \hat{m}_1 < 1.27$

Table 4: *The 95% C.L. ranges of  $\hat{m}_l \equiv M_{\nu QG_l}/M_{\nu QG_l}^{\text{true}}$  obtained using the different dispersion methods and various energy weights for a Monte Carlo simulation of a possible future galactic supernova for  $P = 0.0$ , assuming the normal mass hierarchy and  $M_{\nu QG1} = 10^{10}$  GeV.*

no energy weighting. We see that data from a future galactic supernova could place strong 95% C.L. limits on the range of  $M_{\nu QG2}$  if it is lower than  $10^5$  GeV. In the case of large  $M_{\nu QG2}$ , we find the lower limits  $M_{\nu QG2} > 2.3 \times 10^5$  GeV and  $M_{\nu QG2} > 3.9 \times 10^5$  GeV at the 95% C.L. for subluminal and superluminal models, respectively, in the quadratic case.

Although the ECF method is more sensitive than the MD method, it is not applicable to a statistically poor data set. The ECF method is best for the analysis of a feature in a distribution superposed on a uniform background, and the extraction procedure is possible only with a relatively representative (i.e., large) sample of events. This is demonstrated by simulating a possible future extra galactic supernova which might take place at a distance similar to that of SN 1987a. The simulation has been performed in such a way as to have a sample with sufficient statistics to claim at least a  $3\text{-}\sigma$  detection of Lorentz invariance in neutrino propagation. This would need about 600 events for the linear case, corresponding, assuming the sensitivity of SK, to a supernova at a distance of about 40 kpc from the Earth.

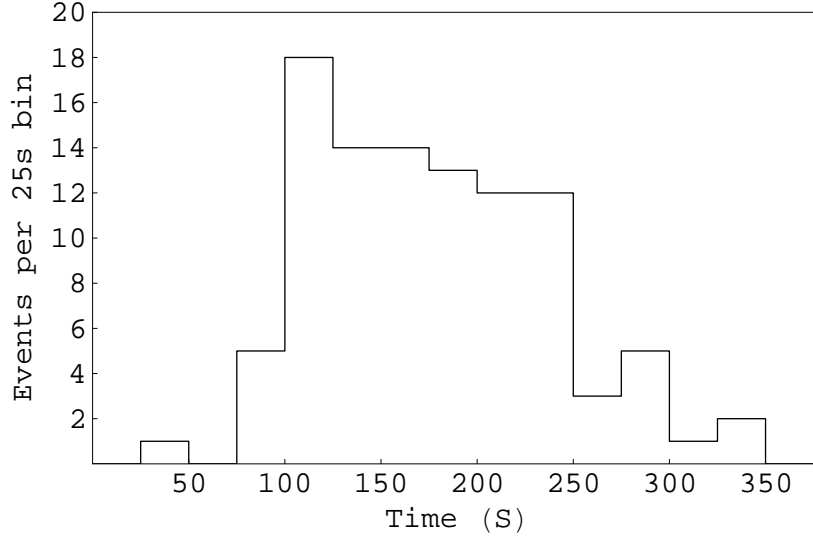


Figure 7: *The time profile of 600 events, which could be detected by SK from a future extra galactic supernovae occurred at the distance 40 kpc from the earth. The events are simulated with respect to the energy spectrum given in Fig. 4 with linear energy depending propagation effect, encoded at the level  $\tau_1 = 5.5 \text{ s} \cdot \text{MeV}^{-1}$ .*

An expected time profile is presented in Fig. 7. The signal Fig. 7 contains 600 events and the time distribution encodes a linearly energy-dependent propagation effect at the level of  $\tau_1 = 5.5 \text{ s} \cdot \text{MeV}^{-1}$ , corresponding to  $M_{\nu QG1} = 7 \times 10^9 \text{ GeV}$ . This distribution does not demonstrate any significant feature that one could extract in a time window to be analyzed using the ECF. Therefore, we apply the MD method, which is better for a signal with poor statistics. The typical behaviour of the dispersion (2) versus  $\tau$  for one realization of the energy-smeared sample of the 600 simulated events is presented in Fig. 8. The distribution of  $\tau_{min}$  given by (4) of 1000 MC simulations similar to Fig. 1 recovers, in this case, the encoded signal  $\tau_1 = 5.5 \text{ s} \cdot \text{MeV}^{-1}$  ( $M_{\nu QG1} = 7 \times 10^9 \text{ GeV}$ ) at the  $3\text{-}\sigma$  level. A similar simulation for the quadratic case would require about 400 events, which would correspond to a SN at a distance of about 50 kpc from the Earth for the SK efficiency. A  $3\text{-}\sigma$  signal could be recovered if the dispersion effect was at the level  $\tau_2 = 0.1 \text{ s} \cdot \text{MeV}^{-2}$ , which corresponds to  $M_{\nu QG2} = 7 \times 10^3 \text{ GeV}$ .

The minimal  $3\text{-}\sigma$  discovery statistics, which amounts to 600 (400) events for linear (quadratic) energy dependence, is defined for the MD method by the uncertainty in the denominator of (4), which reads  $\approx 5/\sqrt{N}$  ( $\approx 4/\sqrt{N}$ ) for either the simulated events or events from SN 1987a, where  $N$  is the number of detected events. This means, that for the statistics of SN 1987a, a Lorentz-violating signal could be detected only at about the  $1\text{-}\sigma$  C.L., corresponding to the bounds obtained in the previous subsection. In the case of limited statistics like SN 1987a, It is possible to estimate similar limits on Lorentz violation without the full MD machinery used in 2.3.1. However, such an estimate would implicitly assumes that the dispersion of the initial signal at the source is known. One could rely on

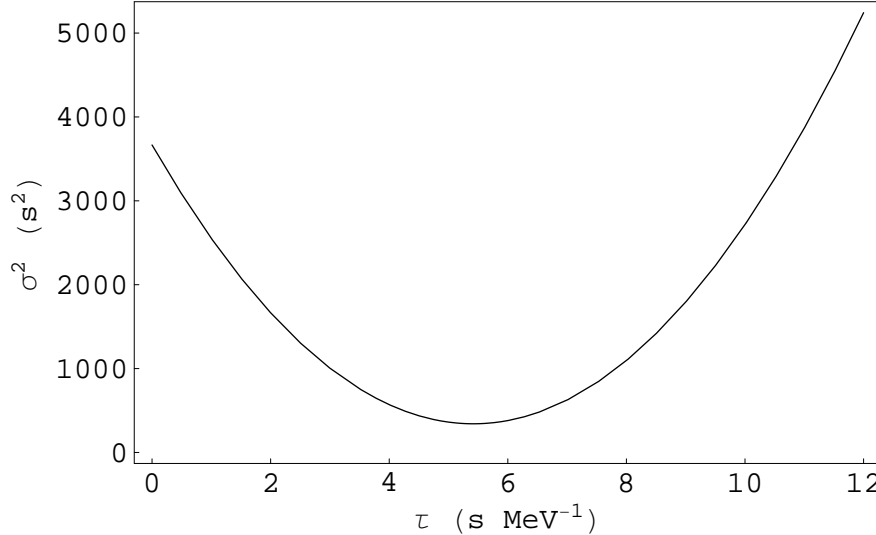


Figure 8: *The dispersion (2) versus  $\tau$  from one realization of the simulated time profile Fig. 7 with neutrino energies smeared by MC applying to the expected energy resolution of SK, for the case of linear energy depending neutrino velocity.*

computer simulations of a supernova explosion [22], but this would introduce an element of model-dependent information into the analysis. The methods considered here do not assume any knowledge on the true profile (spread) of the neutrino signal at the source: instead, they remove any propagation effect that may be encoded in the time profile.

### 3 CNGS and the OPERA Experiment

In this Section we discuss the sensitivities to Lorentz violation in neutrino propagation that could be provided by the OPERA experiment in the CNGS neutrino beam. We first discuss the sensitivity to Lorentz violation that could be obtained using the spill structure alone, without taking into account its bunch substructure. In a second step, we consider how this bunch substructure could be exploited to improve the sensitivity, which could be possible if the timing resolution currently expected for the OPERA detector could be improved significantly.

We first recall some of the details of the pioneering analysis of the neutrino velocity in a long-baseline neutrino beam that has been published by the MINOS collaboration using the NuMI beam [15]. This analysis compared the absolute timings of the detected neutrino events in the near and far detectors. The arrival times in the near detector provide a direct measurement of the neutrino intensity time-profile, consisting of either 5 or 6 batches separated by short gaps within a  $9.7 \mu\text{s}$  long spill. The near and far clocks were synchronized absolutely by means of Global Positioning Satellite (GPS) receivers. The resulting systematic error of  $\pm 64$  ns was dominated by uncertainties in the delays in the optical fibres that ran

Mass hierarchy	95% C.L.
NH $P = 0.0$	$0.90 < \hat{m}_1 < 1.29$
NH $P = 1.0$	$0.90 < \hat{m}_1 < 1.28$
IH $P = 0.0$	$0.91 < \hat{m}_1 < 1.26$
IH SS $P = 0.0$	$0.90 < \hat{m}_1 < 1.27$
IH SS $P = 1.0$	$0.91 < \hat{m}_1 < 1.28$

Table 5: *The 95% C.L. for  $\hat{m}_l \equiv M_{\nu QGl}/M_{\nu QGl}^{true}$  obtained using the ECF method for a Monte Carlo simulation of a possible future galactic supernova, for the normal (NH) and inverted hierarchies (IH), and including the effect of a spectral split (SS), where  $P$  is the level-crossing probability, and NH  $P = 1.0$  is equivalent to IH  $P = 1.0$ .*

Model	95% C.L.
$M_{\nu QG1} = 10^{10}\text{GeV}$	$0.90 < \hat{m}_1 < 1.29$
$M_{\nu QG1} = 10^{11}\text{GeV}$	$0.64 < \hat{m}_1 < 1.93$
$M_{\nu QG1} = 10^{12}\text{GeV}$	$0.22 < \hat{m}_1, 0.42 < \hat{m}_1^{super}$
$M_{\nu QG2} = 10^{4.5}\text{GeV}$	$0.93 < \hat{m}_2 < 1.23$
$M_{\nu QG2} = 10^5\text{GeV}$	$0.65 > \hat{m}_2, 2.3 < \hat{m}_2^{super}$
$M_{\nu QG2} = 10^{5.5}\text{GeV}$	$0.19 > \hat{m}_2, 0.72 < \hat{m}_2^{super}$

Table 6: *The 95% C.L. limits on  $M_{\nu QG1}$  and  $M_{\nu QG2}$  obtained using the KS statistic and the ECF method, for subluminal Lorentz violation with certain input choices of  $M_{\nu QG1}$  (top three rows) and  $M_{\nu QG2}$  (bottom three rows). We give the 95% C.L. limits for subluminal (superluminal) propagation as  $\hat{m}_1$  ( $\hat{m}_1^{super}$ ); if a limit for  $\hat{m}_1^{super}$  is not given then superluminal propagation has been ruled out at the 95% C.L..*

between the surface antennae and the underground detectors. Including the jitter of the two GPS clocks, the total relative time uncertainty was  $\sigma = 150$  ns. This analysis measured  $(v - c)/c = (5.1 \pm 2.9) \times 10^{-5}$  at the 68% C.L., or  $-2.4 \times 10^{-5} < (v - c)/c < 12.6 \times 10^{-5}$  at the 99% C.L., at an average neutrino energy of 3 GeV [15]. In the case of linear Lorentz violation, this would correspond approximately to  $M_{\nu QG1} > 1.2(4.2) \times 10^5$  GeV in the case of subluminal (superluminal) propagation.

### 3.1 CNGS Beam Characteristics

The energy spectrum of the calculated CNGS  $\nu_\mu$  flux is reproduced in Fig. 9. Its average neutrino energy is  $\sim 17$  GeV, significantly higher than that of the NuMI beam. Since the CNGS baseline is almost identical with that of the NuMI beam, this gives some advantage to OPERA, assuming that it can attain similar or better timing properties. We also recall that the CNGS beam is produced by extracting the SPS beam during spills of length  $10.5 \mu\text{s}$  (10500 ns). Within each spill, the beam is extracted in 2100 bunches separated by 5 ns. Each individual spill has a  $4 - \sigma$  duration of 2 ns, corresponding to a Gaussian RMS width



of 0.25 ns [20].

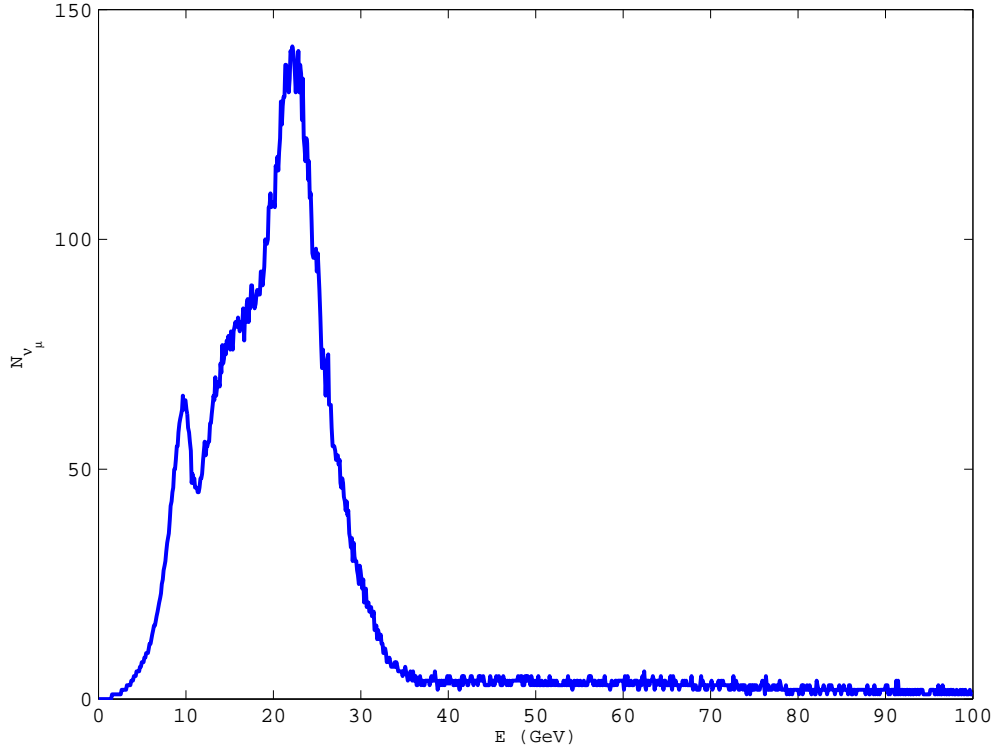


Figure 9: *The expected CNGS neutrino beam energy spectrum [20].*

### 3.2 Spill Analysis

We introduce a ‘slicing estimator’, based on the fact that if some energy-dependent time delay is encoded into the time structure of the spill by propagation of the neutrinos before detection, one should observe a systematic increase in the overall time delay of events as their energies grow. Therefore, we propose cutting the energy spectrum of the neutrino beam into a number of energy slices, and searching for a systematic delay in the mean arrival times of the events belonging to different energy slices that increases with the average energy of the slice.

In order to illustrate this idea, we perform a simple exercise simulating the sensitivity of the slicing estimator for a time delay depending linearly on the neutrino energy:  $\Delta t = \tau E$ , assuming  $\approx 2 \times 10^4$  charged-current events, as are expected to be observed in the 1.8 kton OPERA detector over 5 years of exposure time to the CNGS beam. We envisage superposing all the CNGS spills with a relative timing error  $\delta t$ . Since each spill has 2100 bunches, we expect about 10 events on average due to each set of superposed bunches. As a starting-point, before incorporating the relative timing error, the timing of each event has been smeared using a Gaussian distribution with standard deviation 0.25 ns, reflecting the bunch spread.

We display in Fig. 10 a sample of events in our simulation, before incorporating the relative timing error and any delay in propagation. The 5 ns internal time structure of the spill is clearly visible.

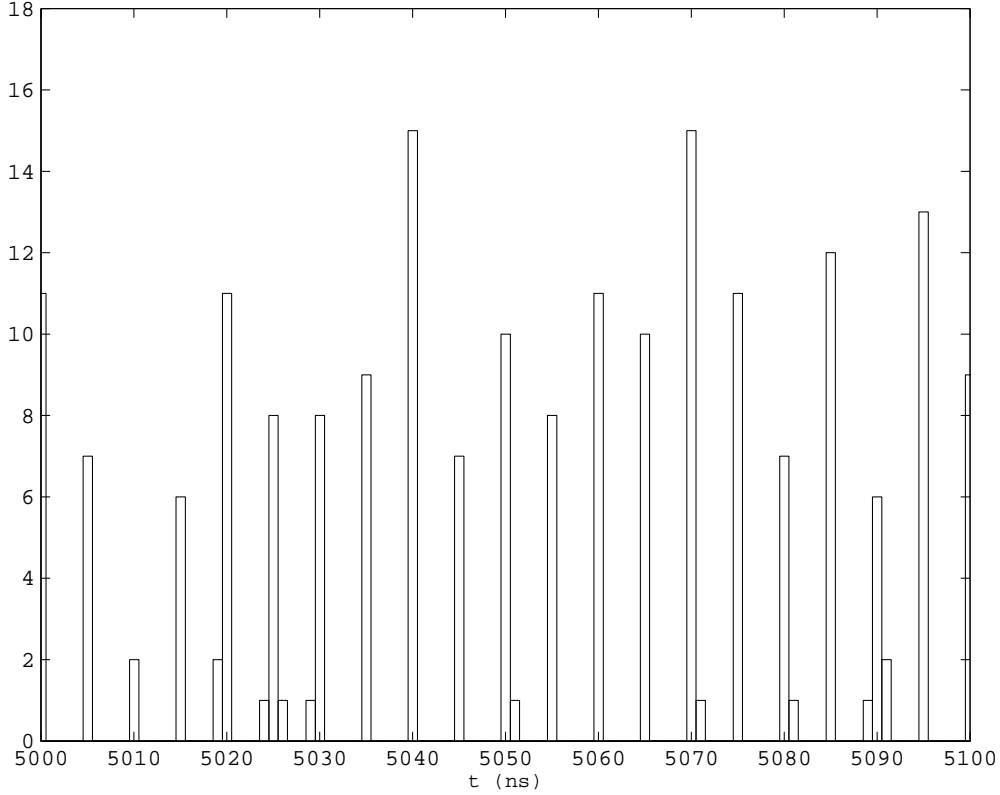


Figure 10: *A superposition of the production times of neutrinos in CNGS spills reflects the bunch structure of the CNGS beam [20].*

We now incorporate the uncertainty in the relative timing of the bunch extraction and the detection of an event in the detector. The overall uncertainty has three components: an uncertainty in the extraction time relative to a standard clock at CERN, an uncertainty in the relative timing of clocks at CERN and the LNGS provided by the GPS system, and the uncertainty in the detector timing relative to a standard clock in the LNGS. With the current beam instrumentation, implementation of GPS and detector resolution, it is expected that this will be similar to that achieved by MINOS in the NuMI beam, namely  $\sim 100$  ns. Such a timing error renders essentially invisible the internal bunch structure of the CNGS spill, which looks indistinguishable from a uniform distribution generated with the same statistics, as shown in the upper panel of Fig. 11.

We next demonstrate in the lower panel of Fig. 11 the effect of a time delay during neutrino propagation at the level of  $\tau_l = 5$  ns/GeV, as would occur if  $M_{\nu_{QG1}} = 4.8 \times 10^5$  GeV. This would correspond to a total delay  $\sim 100$  ns at the average energy of the CNGS neutrino beam. We see clearly its smearing effect at the beginning and end of the spill, due to the

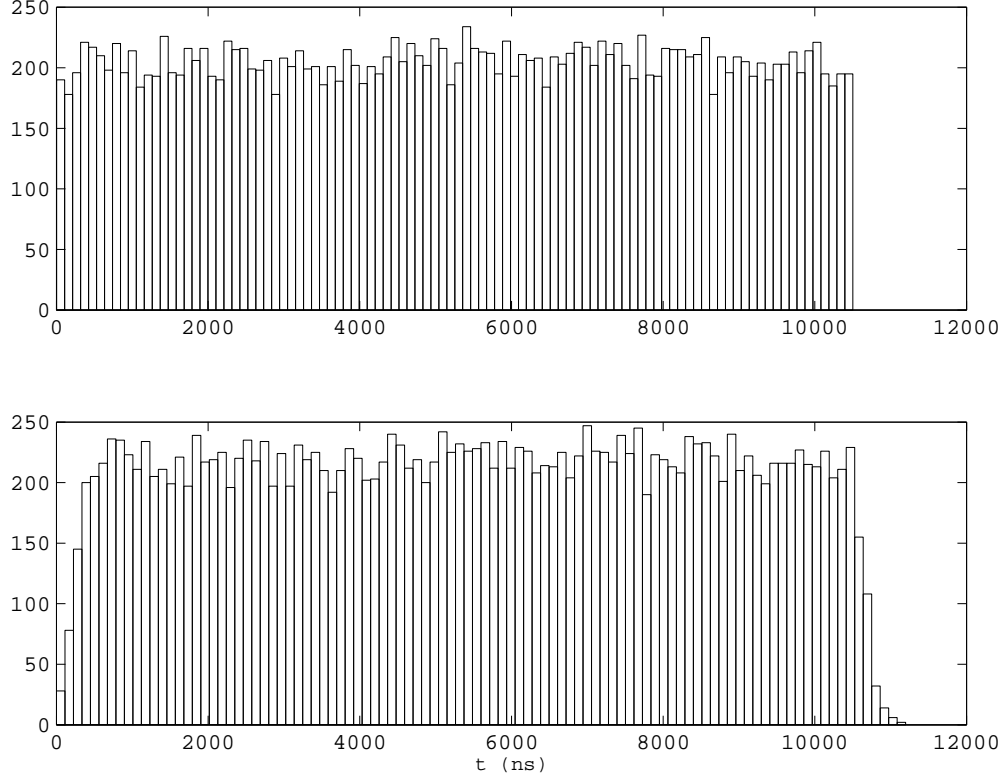


Figure 11: *The time structure of events in the CNGS beam, including a 100 ns timing uncertainty without (upper panel) Lorentz violation in neutrino propagation, and (lower panel) with a linearly energy-dependent time delay during neutrino propagation at the level of  $\tau = 5 \text{ ns/GeV}$ .*

later arrivals of the more energetic neutrinos. Our ‘slicing estimator’ aims to quantify this effect.

We smear the events with an energy resolution of 20%, and then cut the sample into slices of about 1000 events each with increasing energies. The asterisks in Fig. 12 show the mean arrival times of each slice, relative to the mean time of the superposed spills, using one particular smearing of the timing with a Gaussian error  $\delta t = 100 \text{ ns}$ . The triangles in Fig. 12, on the other hand, show the mean arrival times of events in each energy slice if the propagation delays caused by an assumed value of  $\tau = 5 \text{ ns/GeV}$  are included. We see clear differences between the asterisks and the red and triangles, that increase with the energies of the slices.

By making many realizations of the event sample with the Gaussian  $\delta t = 100 \text{ ns}$  smearing, one can understand the significance of the shifts in the mean positions of the slices. Fig. 13 shows the energy dependence of the shifts in the mean timings of the slices of 1000 events with a delay  $\tau_l = 5 \text{ ns/GeV}$  encoded. These points may be fitted to a straight line

$$\Delta\langle t \rangle = \tau_l \langle E \rangle + b. \quad (8)$$

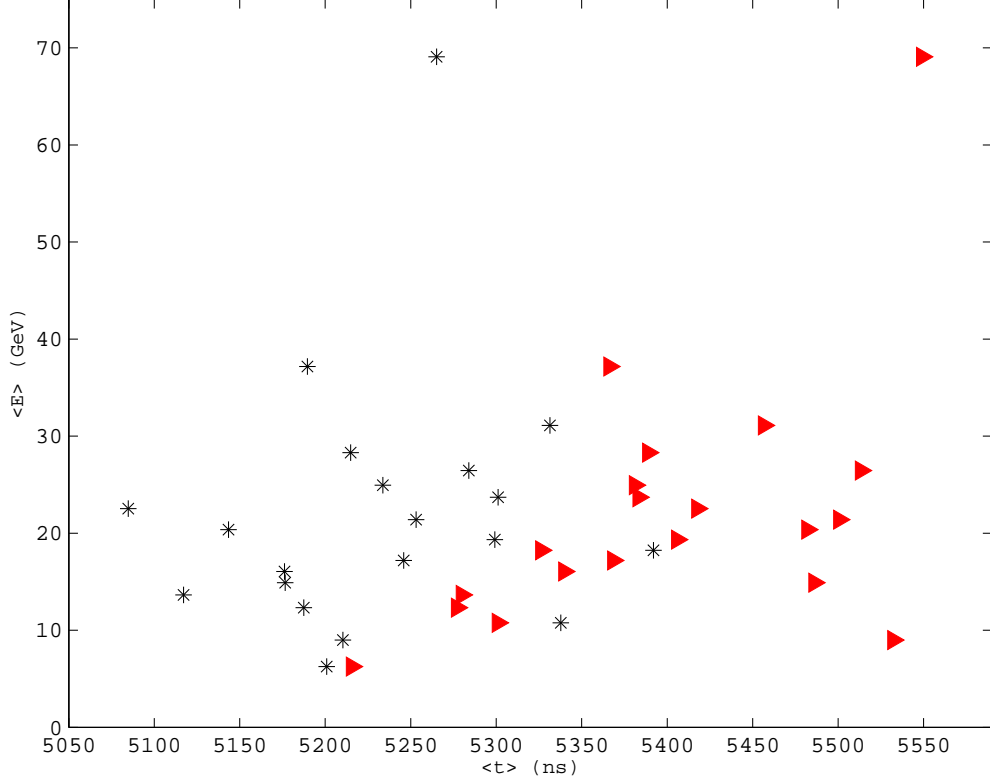


Figure 12: *The mean arrival times of 1000-event slices with increasing energies without Lorentz violation in the neutrino propagation (asterisks) and with the effect of a time delay during neutrino propagation at the level of  $\tau = 5 \text{ ns/GeV}$  (triangles). The latter corresponds to  $M_{\nu QG1} = 4.8 \times 10^5 \text{ GeV}$ . One particular simulation of the OPERA experiment is shown: others are similar, exhibiting the expected statistical fluctuations.*

In general, when choosing the number of events for each slice, one has to strike a balance between the statistics of each subsample (which determines the precision of the determination of the mean arrival time of each slice), and the number of subsamples to be included in the fit. We choose the statistics of each slice so as to give comparable error bars for each energy bin. The propagation effect of interest to us is reflected in the slope  $\tau_l$ , while the intercept is an overall shift that has no physical significance. The sensitivity of the experiment to linear Lorentz violation at, say, the 95% confidence level (C.L.) may be estimated by finding the value of the parameter  $\tau_l$  which yields a fitted slope parameter that differs from a horizontal line ( $\tau_l = 0$ ) by  $1.95\sigma$  or more. We show in Fig. 14 the confidence contours corresponding to 68%, 95% and 99% sensitivity levels in the  $(b, \tau_l)$  plane. From the upper (lower) edge of the corresponding ellipse one obtains  $\tau_{l95\%} = 4.9(2.6) \text{ ns/GeV}$  at the 95% C.L. for the subluminal (superluminal) propagation schemes, corresponding via

$$M_{\nu QG1} = \frac{L_{\text{CNGS}}}{c} \tau_l^{-1} = 2.4 \times 10^6 \left( \frac{\text{ns GeV}^{-1}}{\tau_l} \right) \text{ GeV} \quad (9)$$

to values of the linear Lorentz-violating scale  $M_{\nu QG1} = 4.9(9.2) \times 10^5$  GeV for the subluminal (superluminal) case, yielding a mean sensitivity<sup>5</sup> to  $M_{\nu QG1} \simeq 7 \times 10^5$  GeV. It is important

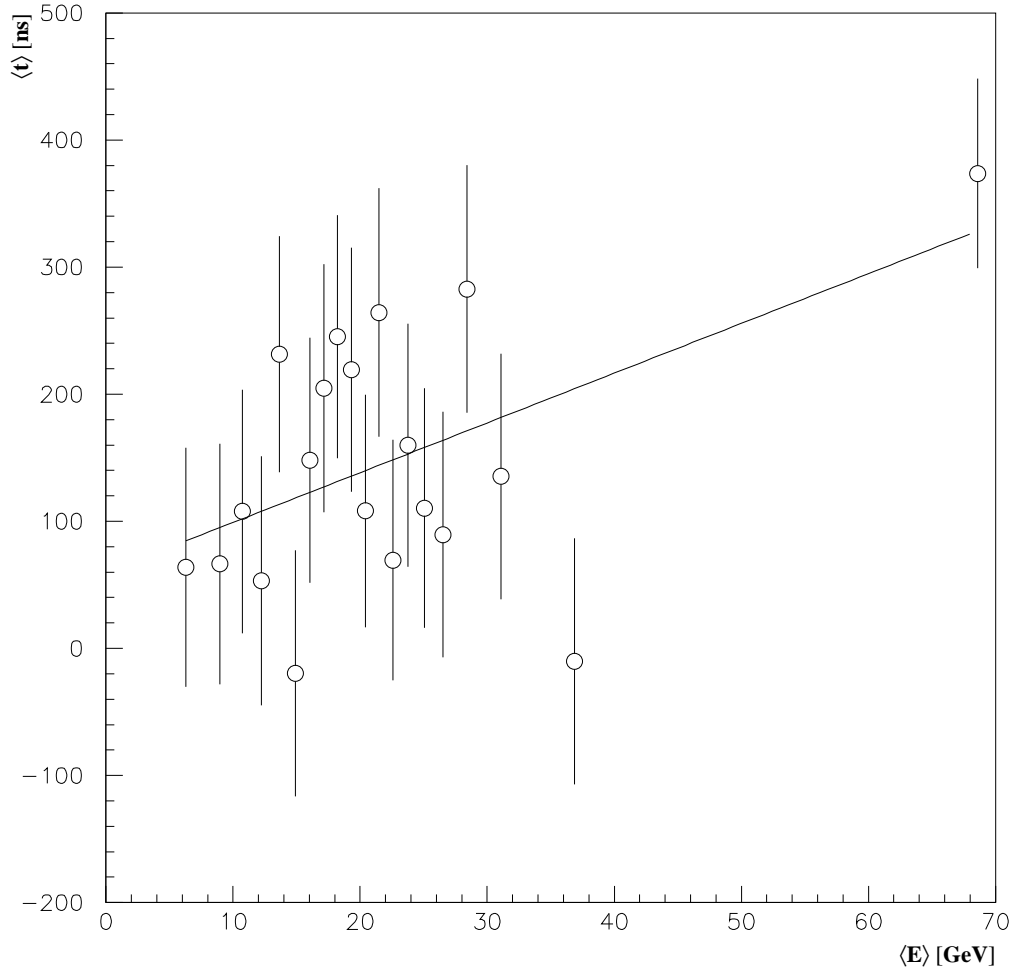


Figure 13: *The measured shifts in the average arrival times of neutrinos in 1000-event slices with increasing energies, assuming a time delay during neutrino propagation at the level of  $\tau = 5$  ns/GeV.*

to note that the slope and intercept are anticorrelated in such a fit, as shown in Fig. 14. Our conservative estimate of the limits corresponds to the upper (lower) edges of the ellipse.

If the velocity of the neutrino depends quadratically on the energy of the neutrino, the slices should obey a parabolic fit

$$\Delta\langle t \rangle = \tau_q \langle E \rangle^2 + c. \quad (10)$$

---

<sup>5</sup>Since the CNGS spill is in principle time symmetric, the estimated sensitivities for sub- and superluminal propagation should be the same. The difference between these numbers reflects the finite size of the simulated sample. Here and subsequently we quote the means of our sum and superluminal limits as estimates of the CNGS sensitivity.

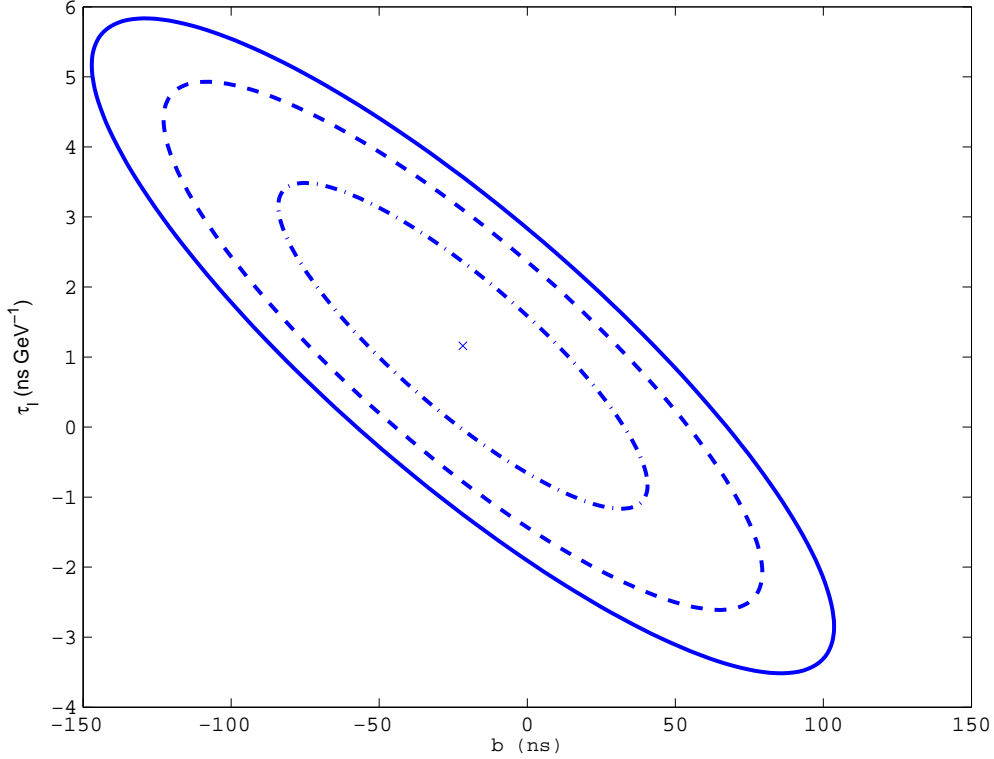


Figure 14: The 68% (dashed dotted line), 95% (dashed line) and 99% (solid line) sensitivity contours for the case of linear energy-dependent fit (8).

Here the propagation effect of interest is parameterized by  $\tau_q$ , while an overall shift is reflected in the constant  $c$ . The sensitivity contours at 68% , 95% and 99% CL are presented in Fig. 15. According to the formula

$$M_{\nu QG2} = \sqrt{\frac{L_{\text{CNGS}}}{c} \tau_q^{-1}} = 1.6 \times 10^3 \sqrt{\frac{ns \text{ GeV}^{-2}}{\tau_q}} \text{ GeV}, \quad (11)$$

after substituting  $\tau_{q95\%} = 0.066(0.022)$ , we obtain  $M_{\nu QG1} = 6.2(11) \times 10^3 \text{ GeV} \simeq 8 \times 10^3 \text{ GeV}$ .

The stability of the slicing estimator has been checked by generating several data sets that have linear or quadratic dispersion effects artificially encoded. To test our level of sensitivity, we chose the Lorentz-violating parameters to be close to our estimations of the levels of sensitivities in the case of where dispersion effects are absent. The encoded values have been recovered for the linear (8) and quadratic (10) fits to slices containing the same numbers of events. Slight variations in the numbers of events in the individual slices do not change substantially the levels of sensitivity estimated for 1000-event bins. Another check has been performed using the minimal dispersion method described in Section 2.2.1. This method has been applied to the whole sample of about  $2 \times 10^5$  events expected to occur in the rock upstream of the OPERA detector, and results very similar to those of the slicing

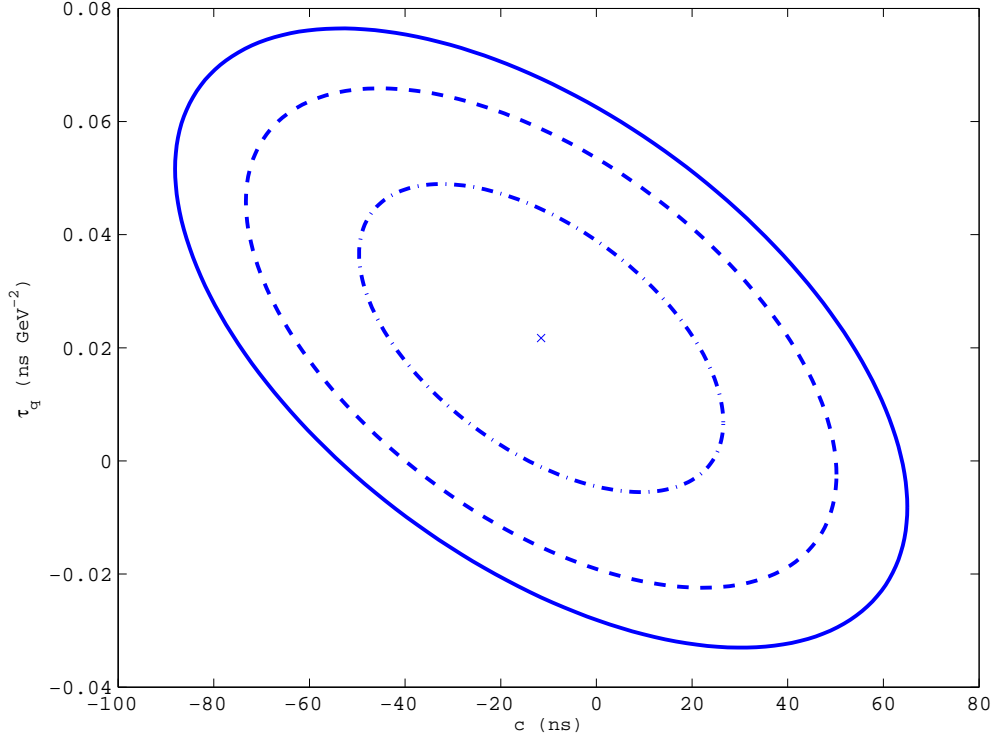


Figure 15: *The same as in Fig. 14 calculated for the sensitivity of the quadratically energy-dependent fit (10).*

estimator have been obtained. Although the whole data sample is very rich statistically, the time distribution, given the 100 ns time uncertainty assumed in the current analysis, is still featureless apart the edges of the spill <sup>6</sup>.

Another check has been made analyzing the distortion of the shape of the spill at its edges. For this purpose, we analyze two independent histograms of the type shown in Fig. 11. One of the histograms is treated as a reference, while the other was shifted by introducing a time delay  $\tau_{l(q)}$  for every event, corresponding to the linear (quadratic) propagation scheme. The shifted histogram has been compared to the reference (unshifted) histogram, and the parameter  $\tau_{l(q)}$  increased until the difference between two histograms reaches the 95% C.L. We find that this edge-fitting method has a factor 5 less sensitivity than that obtained earlier with the slicing estimator or the MD method.

We recall that the OPERA detector may also be used to measure the arrival times of muons from  $2 \times 10^5$  neutrino events in the rock upstream of the detector. Information on the neutrino energy is missing in this measurement. Therefore, one cannot employ methods involving time-energy correlation information such as the slicing estimator. Methods requiring an energy-dependent time shift of the data, like the MD method, are also not applicable in this case, again because events in the rock do not have measured energies. Nevertheless, one

---

<sup>6</sup>For this reason, the ECF technique described in Section 2 is inapplicable.

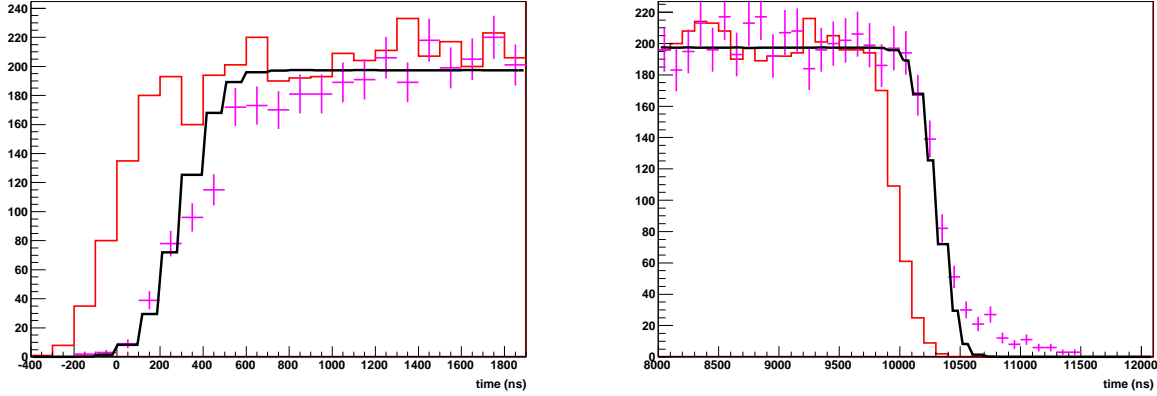


Figure 16: *The left (right) spill edges fitted using 20000 detector events for scenario with a linear energy dependence of the neutrino velocity. The solid red line is the reference histogram, while the points represent the shifted data. The solid black line represents the probability distribution function.*

can use methods that compare overall the time shift of the simulated data to the measured time distribution of the rock events. In this spirit, applying to the  $2 \times 10^5$  expected rock events the edge-fitting procedure described in the previous paragraph, we find a sensitivity to  $M_{\nu QG1} \approx 2.4 \times 10^6$  GeV, about three times better than previously, for the sensitivity to linear energy dependence, and the same level of sensitivity for the quadratic energy dependence.

One can also modify the MD method for analyzing rock events. Namely, one could generate the reference spill and introduce an energy-dependent shift via the parameter  $\tau_{l(q)}$  so as to make the dispersion of the shifted reference spill match as closely as possible the dispersion of the events measured in the rocks. However, due to statistical uncertainties the dispersion of each reference spill will be different to the dispersion of the rock events. If this uncertainty is much less than the increase in the dispersion of the rock events due to Lorentz violation then this method can be used. However, this limits the sensitivity to  $M_{\nu QG1} \simeq 3 \times 10^5$  GeV for the linear propagation scheme, which is not as sensitive to other methods we have described above. From the other side the sensitivity of this modified MD method approaches to  $M_{\nu QG2} \simeq 7 \times 10^3$  GeV, which is similar to the slicing estimator.

### 3.3 Bunch Analysis

We now explore the additional sensitivity that OPERA could obtain if it could achieve a correlation between the SPS RF bunch structure and the detector at the nanosecond level. Sub-ns resolution could be obtained in OPERA with the help of additional specialized timing detectors such as TOF hodoscopes <sup>7</sup>. However, synchronizing the SPS and OPERA

---

<sup>7</sup>We point out that it is sufficient to refer all measured far times to a well-defined plane perpendicular to the beam axis.



clocks with such a precision over a period of 5 years is a challenging task. With the new IEEE Standard Precision Time Protocol (PTP) IEEE1588 [34] it is possible to achieve time synchronization in the range of 100 ns on an Ethernet network but not better; GPS clock synchronization at the ns level is also highly demanding. Standard ‘One-Way’ GPS techniques [35] can reach a precision of  $\sim 20$  ns at best. Devices known as GPS disciplined oscillations (GPSDO) [36], containing high-quality temperature-controlled local oscillators, steered to agree with the onboard oscillators of the GPS satellites, can provide ultra-precise standard frequencies that could reproduce the CERN RF frequency. A more elegant but less standard method is called ‘Common-View’ GPS [35]: in this case two clocks (e.g., one at CERN and the other at LNGS) view simultaneously the same GPS satellite, thereby cancelling out the common errors (e.g., the satellite’s local clock). It has been shown that the data recorded by the two GPS receivers can be processed offline to provide a timing uncertainty  $\lesssim 5$  ns. Finally it has been shown that ‘Carrier-Phase’ GPS measurements [37], which use the carrier frequencies instead of the codes transmitted by the satellites, can achieve synchronization of clocks with uncertainties  $\sim 0.5$  ns at the cost of extensive post processing. Turning to ground based solutions, the most precise atomic clock (the NIST-F1 used to define the UTC) has a long-term accuracy of  $5 \times 10^{-16}$  or  $\sim 75$  ns over 5 years. It would therefore not be sufficient to bring two *a priori* synchronized clocks to the near and far locations to define the arrival times with the required long-term stability. Alternatively, next-generation accelerators, e.g., free electron lasers such as XFELs that aim to generate X-ray pulses with pulse durations down to tens of femtoseconds, will meet the challenge of finding new methods of ultra-stable timing stabilization, synchronization and distribution over several kilometres. These systems will most likely rely on optical timing synchronization. We can therefore imagine a phase-locked loop RF oscillator located at the far location remotely locked to the SPS RF system. These two systems would be connected and locked via stabilized optical fibre links<sup>8</sup>. To conclude, a combination of space- or ground-based solutions could probably provide the possible synchronization of the CNGS and OPERA clocks, and allow for systematic cross-checks to be performed.

We now discuss how the sensitivity of the previous analysis could be improved by taking into account the 5-ns bunch structure of the CNGS spills. In Fig. 17 we present one particular realization of a sample of simulated events which incorporates a relative timing error of 1 ns. Although the periodic bunch structure survives, the signal itself represents a time series with a relatively low signal-to-noise ratio. The latter implies that the proper deconvolution to extract isolated features cannot be made. In other words, there is a problem in fitting the fine structure of the signal with an analytical function. Such a situation has been widely investigated and applied to the temporal profiles of gamma gamma ray bursters (GRBs) [38]. We therefore apply a cross correlation function (CCF) method similar to that described in [38] but differing only in details of its adaptation. Namely, we introduce the

---

<sup>8</sup>We note that the temperature dependence of the refractive index of an optical fibre is typically  $10^{-6}/\text{K}$ , which corresponds to a drift of 5 ns for 1000 km and a temperature stability of  $1^\circ\text{C}$ .

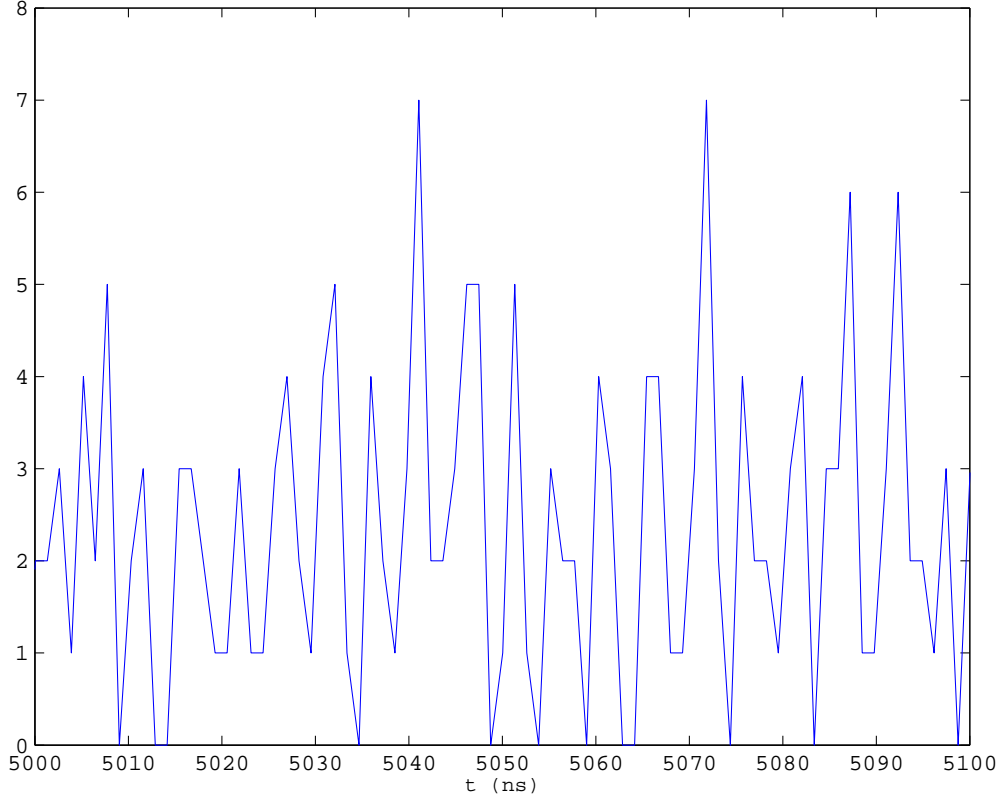


Figure 17: *A particular realization of the bunch structure with  $\approx 1$  ns relative time uncertainty incorporated. The histogram is binned with a resolution suitable for resolving the bunch structure.*

temporal correlation of two time series  $A(t)$  and  $B(t + \tau_{l(q)})$

$$\text{CCF}(\tau_{l(q)}) = \frac{\langle (A(t) - \bar{A}(t))(B(t - \tau_l E^l) - \bar{B}(t - \tau_l E^l)) \rangle}{\sigma_{A(t)} \sigma_{B(t - \tau_l E^l)}}, \quad (12)$$

where  $A(t)$  is a Monte Carlo simulation of the events with no dispersion effects,  $B(t - \tau_l E^l)$  is the simulated data which has the time shift required to invert the effect of the energy-dependent dispersion,  $\bar{A}(t)$  and  $\bar{B}(t - \tau_l E^l)$  are the mean values of the corresponding time series, and  $\sigma_{A(t)}$  and  $\sigma_{B(t - \tau_l E^l)}$  are the standard deviations from these mean values. We average over several Monte Carlo simulations to include the statistical uncertainties as well as performing time and energy smearing due to the uncertainty in these measurements.

We calculate the  $\text{CCF}(\tau_{l(q)})$  as a function of  $\tau_l$  and find its maximum value. The value of  $\tau_l$  which maximizes the CCF is an estimate of the true value of  $\tau_l$ . To find this estimate we fit a Gaussian to the peak of the resulting CCF function shown in Fig. 18. Each realization produced an independent measurement of the CCF at a given value of the shift parameter. The process of iteration for every value of the shift parameter in Fig. 18 was repeated until the resulting distribution approached a normal distribution, which typically took about 100

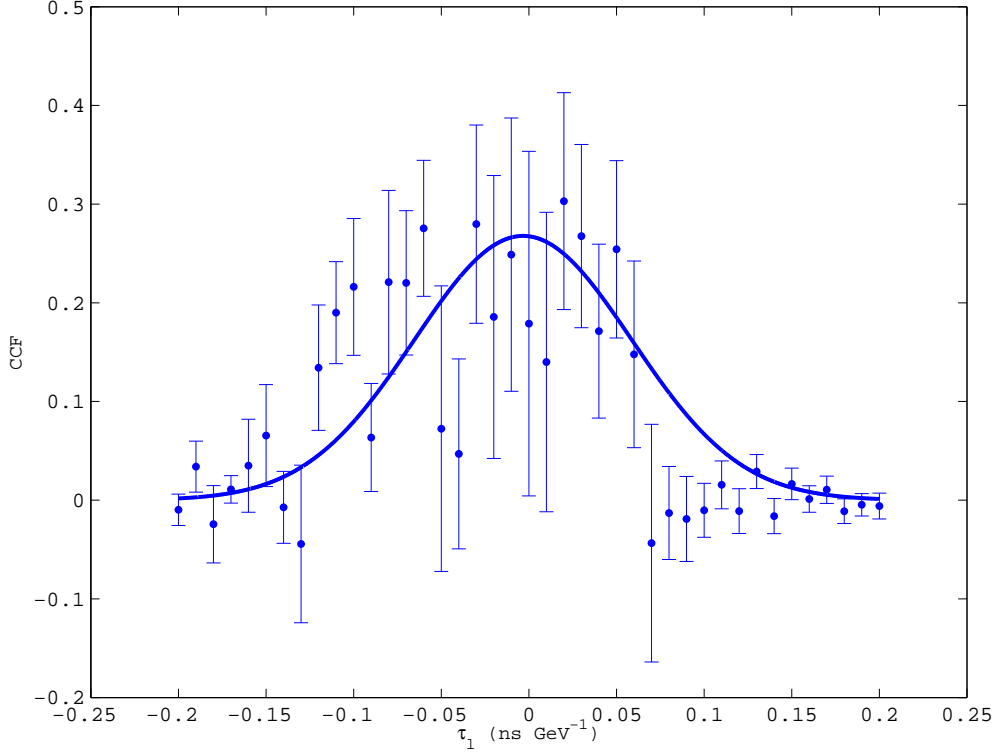


Figure 18: *The Gaussian fit to the CCF calculated for the case of a linear energy dependence with time smearing  $\approx 1$  ns.*

runs. Using these normal distributions the values and the standard deviations (error bars) presented in Fig. 18 have been calculated.

The sensitivity of the CCF can then be estimated by the precision of the position of the maximum for the Gaussian fit in Fig. 18. For the case of linear energy dispersion, the maximum of the CCF is found at  $\tau_1^{\max} = -0.033 \pm 0.036$  ns/GeV if no time shift encoded in the simulated data. For superluminal propagation, when  $\tau_1 > 0$ , one can estimate  $\tau_{195\%}^{\text{su}} = 0.037$  ns/GeV, which corresponds via (9) to  $M_{\nu QG1} \approx 6.6 \times 10^7$  GeV. For the subluminal case, one obtains  $\tau_{195\%}^{\text{sb}} = 0.1$  ns/GeV, which corresponds to  $M_{\nu QG1} \approx 2.4 \times 10^7$  GeV. The same CCF procedure may also be applied to the quadratic case, as shown in Fig. 19. The limits deduced from the fit Fig. 19 are  $M_{\nu QG2} = 3.6(4.9) \times 10^4$  GeV  $\simeq 4 \times 10^4$  GeV.

Repeating the CCF procedure for a time resolution above 2 ns, one observes no maximum correlation in a reasonable range of the shift parameter, as seen in Fig. 20. From this one can conclude that the bunch structure degenerates into an essentially uniform distribution as soon as the time resolution becomes bigger than  $\approx 2$  ns, in which case the slicing estimator described in the previous subsection should be applied.

If the same time resolution  $\sim 1$  ns can be attained for events occurring in the rock upstream from the OPERA detector, the CCF method can also be used to analyze these data, which should amount to some  $2 \times 10^5$  events. We see in Fig. 21 that the bunch structure

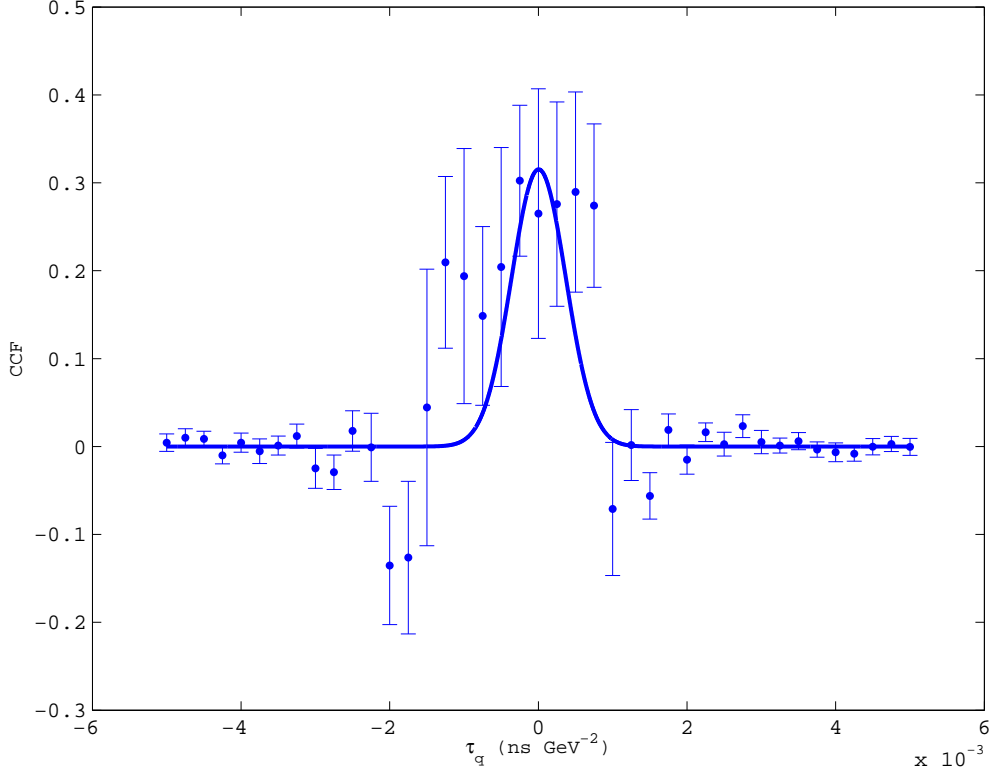


Figure 19: *The same as in Fig. 18 for the quadratic energy dependence.*

of the rock events is clearly visible if a time resolution  $\approx 1$  ns is achieved, despite the fact that the energies of the neutrinos colliding in the rock cannot be determined. The CCF calculated for the rock events is presented in Fig. 22, together with a Gaussian fit. The sensitivities to Lorentz violation now attain the levels of  $M_{\nu QG1} = 4.3(3.2) \times 10^8$  GeV  $\simeq 4 \times 10^8$  GeV for the linear case, and  $M_{\nu QG2} = 8.8(4.3) \times 10^5$  GeV  $\simeq 7 \times 10^5$  GeV for the quadratic case. The sensitivity in the quadratic case is significantly better than the sensitivity estimated for a possible future galactic supernova.

## 4 Conclusions

We find from the SN1987a data lower limits on the scale of linear Lorentz violation in the neutrino sector, namely  $M_{\nu QG1} > 2.68 \times 10^{10}$  GeV and  $M_{\nu QG1} > 2.51 \times 10^{10}$  GeV at the 95% C.L. in the subluminal and superluminal cases respectively. The corresponding limits for the quadratic models are  $M_{\nu QG2} > 4.62 \times 10^4$  GeV and  $M_{\nu QG2} > 4.13 \times 10^4$  GeV at the 95% C.L. in the subluminal and superluminal cases, respectively. We have also used a Monte Carlo simulation of a galactic supernova at 10 kpc to estimate how accurately Lorentz violation could be probed in the future. In such a case one would observe more events because of the larger fiducial volume of the SK detector compared to the previous generation of

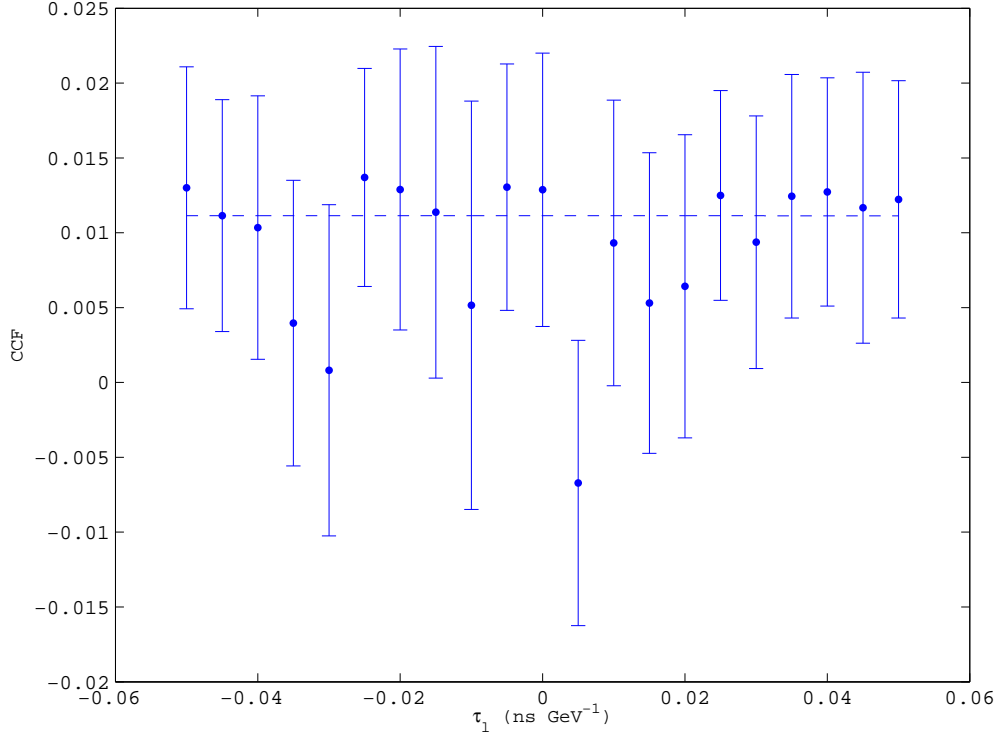


Figure 20: *The profile of the CCF calculated with a 2 ns time resolution for the case of linear energy dependence in neutrino propagation.*

detectors, and because the next observable supernova is likely to be inside the galaxy and hence closer than SN1987a. On the other hand, if the next supernova is closer than SN1987a then the energy-dependent time shift due to Lorentz violation will be reduced, reducing also the expected sensitivity. We performed simulations for both the normal and inverted mass hierarchies and for both an adiabatic and a non-adiabatic atmospheric resonance. In all scenarios it would be possible to probe Lorentz violation using the methods described in this paper. We used the minimal dispersion (MD) method and the maximal ECF method with a several energy weightings and have shown that using the latter with a linear energy weighting has the greatest sensitivity. Using this method we have shown that we could place limits up to  $M_{\nu QG1} > 2.2 \times 10^{11}$  GeV and  $M_{\nu QG1} > 4.2 \times 10^{11}$  GeV at the 95% C.L. for the subluminal and superluminal cases, respectively, for linear models of Lorentz violation, and  $M_{\nu QG2} > 2.3 \times 10^5$  GeV and  $M_{\nu QG2} > 3.9 \times 10^5$  GeV at the 95% C.L. for the subluminal and superluminal cases, respectively, for quadratic models of Lorentz violation.

We have then explored the sensitivity to Lorentz violation in neutrino propagation that could be obtained using data from the OPERA detector in the CNGS beam. By comparison with the result already obtained by MINOS in the NuMI beam, OPERA would benefit from the higher energy of the CNGS beam, the larger statistics we assume, and the possibility of exploiting the bunch structure of the CNGS beam that we have explored. We find that,

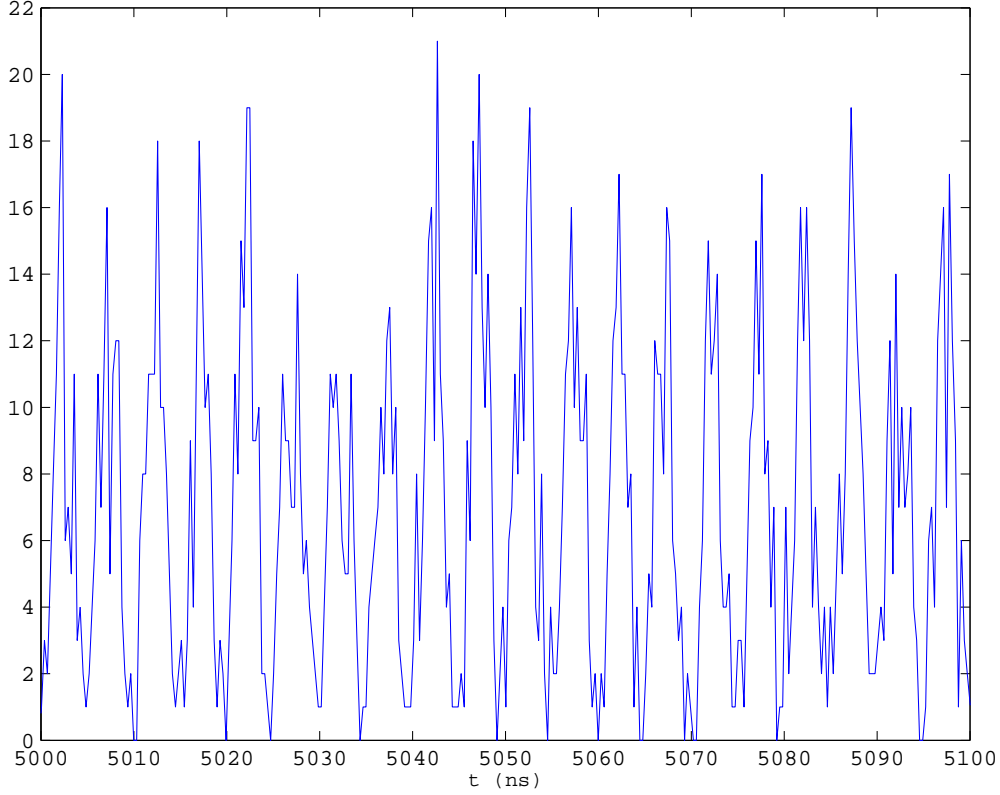


Figure 21: *A simulated realization of the bunch structure for rock events, incorporating a timing uncertainty  $\approx 1$  ns. The histogram is binned with a resolution suitable for resolving the bunch structure.*

using standard clock synchronization techniques, the sensitivity of the OPERA experiment would reach  $M_{\nu_{QG1}} \sim 7 \times 10^5$  GeV ( $M_{\nu_{QG2}} \sim 8 \times 10^3$  GeV) after 5 years of nominal running. If the time structure of the SPS RF bunches within the extracted CNGS spills of  $10.5 \mu\text{s}$  could be exploited, which would require reducing the timing uncertainty to  $\sim 1$  ns, these figures would be significantly improved to  $M_{\nu_{QG1}} \sim 5 \times 10^7$  GeV ( $M_{\nu_{QG2}} \sim 4 \times 10^4$  GeV). Using events in the rock upstream of OPERA, and again assuming a time resolution  $\sim 1$  ns, the sensitivities to Lorentz violation could be further improved to  $M_{\nu_{QG1}} \simeq 4 \times 10^8$  GeV for the linear case and  $M_{\nu_{QG2}} \simeq 7 \times 10^5$  GeV for the quadratic case. While still inferior to the sensitivity of the supernova limits in the linear case, the OPERA rock sensitivity in the quadratic case would exceed even that possible using data from a future galactic supernova. This and the fact that any accelerator limit benefits from better-understood experimental conditions would motivate the effort that would be required to achieve nanosecond time resolution for the OPERA/CNGS combination.

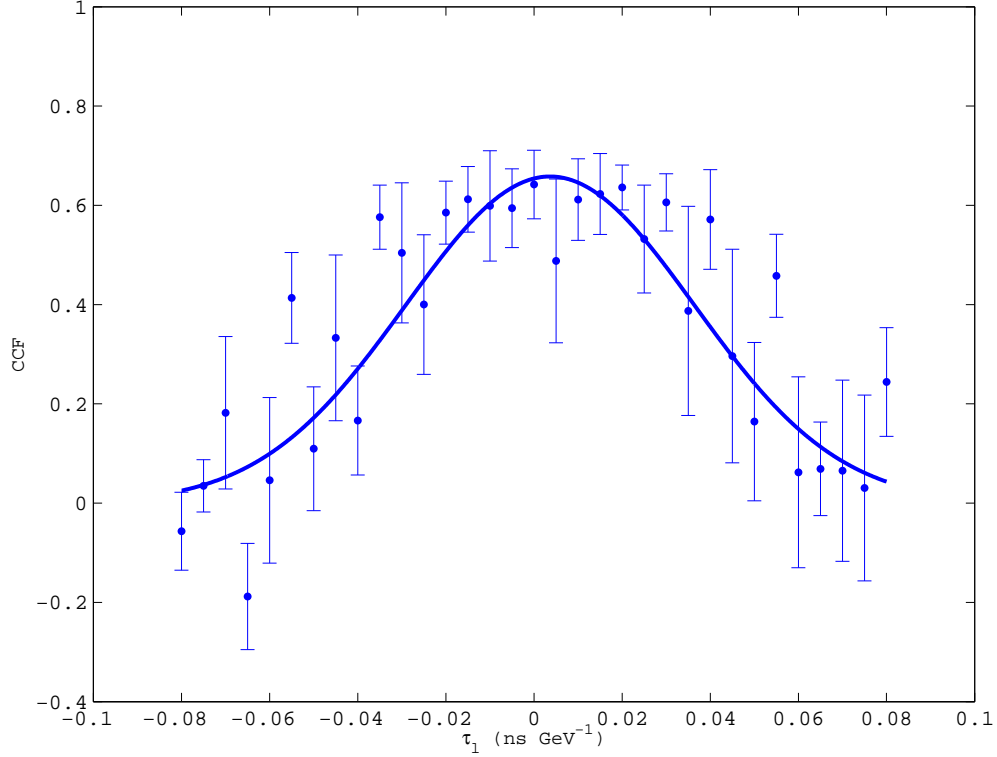


Figure 22: *The CCF for rock events with time resolution  $\approx 1$  ns in the case of linear energy dependence, compared with a Gaussian fit.*

## Acknowledgements

We thank N. E. Mavromatos, D. V. Nanopoulos and E. K. G. Sarkisyan for discussions on related subjects. N. H. and A. S. S. thank the CERN Theory Division for its kind hospitality. N. H. also thanks STFC for the Studentship Award PPA/S/S/2004/03926, and the UniverseNet network for supporting this research project by a Marie Curie Early Stage Research Training Fellowship of the European Community's Sixth Framework Programme under contract (MRTN-CT-2006-0355863-UniverseNet).

## References

- [1] For reviews, see: A. Strumia and F. Vissani, arXiv:hep-ph/0606054.
- [2] Y. Totsuka, Rept. Prog. Phys. **55** (1992) 377.
- [3] G. Barenboim, N. E. Mavromatos, S. Sarkar and A. Waldron-Lauda, Nucl. Phys. B **758** (2006) 90 [arXiv:hep-ph/0603028].

- [4] N. E. Mavromatos, A. Meregaglia, A. Rubbia, A. Sakharov and S. Sarkar, Phys. Rev. D **77** (2008) 053014 [arXiv:0801.0872 [hep-ph]].
- [5] D. Morgan, E. Winstanley, J. Brunner and L. F. Thompson, Astropart. Phys. **25** (2006) 311 [arXiv:astro-ph/0412618].
- [6] D. Hooper, D. Morgan and E. Winstanley, Phys. Lett. B **609** (2005) 206 [arXiv:hep-ph/0410094].
- [7] G. Amelino-Camelia, J. R. Ellis, N. E. Mavromatos and D. V. Nanopoulos, Int. J. Mod. Phys. A **12** (1997) 607 [arXiv:hep-th/9605211]; J. R. Ellis, N. E. Mavromatos and D. V. Nanopoulos, Phys. Lett. B **293** (1992) 37 [arXiv:hep-th/9207103]; J. R. Ellis, N. E. Mavromatos and D. V. Nanopoulos, *Erice Subnucl. Phys. Series*, Vol. **31** 1 (World Sci. 1994) [arXiv:hep-th/9311148]; J. Chaos, Solitons and Fractals, Vol. **10** (1999) 345 (eds. C. Castro and M.S. El Naschie, Elsevier Science, Pergamon 1999) [arXiv:hep-th/9805120];
- [8] R. Gambini and J. Pullin, Phys. Rev. D **59** (1999) 124021 [arXiv:gr-qc/9809038]; J. Alfaro, H. A. Morales-Tecotl and L. F. Urrutia, Phys. Rev. D **65** (2002) 103509 [arXiv:hep-th/0108061]; V. A. Kostelecky and S. Samuel, Phys. Rev. D **39** (1989) 683; G. Amelino-Camelia, Int. J. Mod. Phys. D **11** (2002) 35 [arXiv:gr-qc/0012051]; R. C. Myers and M. Pospelov, Phys. Rev. Lett. **90** (2003) 211601 [arXiv:hep-ph/0301124].
- [9] G. Amelino-Camelia, J. Ellis, N. Mavromatos, D. Nanopoulos and S. Sarkar, Nature **393** (1998) 763; J. Ellis, K. Farakos, N.E. Mavromatos, V.A. Mitsou and D.V. Nanopoulos, Ap. J. **535** (2000) 139; J. R. Ellis, N. E. Mavromatos, D. V. Nanopoulos, A. S. Sakharov and E. K. G. Sarkisyan, Astropart. Phys. **25** (2006) 402 [Astropart. Phys. **29** (2008) 158] [arXiv:astro-ph/0510172]; *ibid* J. Ellis, N. E. Mavromatos, D. V. Nanopoulos, A. S. Sakharov and E. K. G. Sarkisyan, arXiv:0712.2781 [astro-ph].
- [10] P. Kaaret, Astron. Astrophys. **345** (1999) L32 [astro-ph/9903464].
- [11] J. Albert *et al.* [MAGIC Collaboration], arXiv:0708.2889 [astro-ph].
- [12] J. R. Ellis, N. E. Mavromatos, D. V. Nanopoulos and A. S. Sakharov, Int. J. Mod. Phys. A **19** (2004) 4413 [arXiv:gr-qc/0312044].
- [13] J. Ellis, N. E. Mavromatos and D. V. Nanopoulos, arXiv:0804.3566 [hep-th].
- [14] J. R. Ellis, N. E. Mavromatos, D. V. Nanopoulos and G. Volkov, Gen. Rel. Grav. **32**, 1777 (2000) [arXiv:gr-qc/9911055].
- [15] P. Adamson *et al.* [MINOS Collaboration], Phys. Rev. D **76** (2007) 072005 [arXiv:0706.0437 [hep-ex]].



- [16] R. M. Bionta *et al.*, Phys. Rev. Lett. **58** (1987) 1494.
- [17] K. Hirata *et al.* [KAMIOKANDE-II Collaboration], Phys. Rev. Lett. **58** (1987) 1490.
- [18] E. N. Alekseev, L. N. Alekseeva, V. I. Volchenko and I. V. Krivosheina, JETP Lett. **45** (1987) 589 [Pisma Zh. Eksp. Teor. Fiz. **45** (1987) 461].  
E. N. Alekseev, L. N. Alekseeva, I. V. Krivosheina and V. I. Volchenko, Phys. Lett. B **205** (1988) 209.
- [19] V. Ammosov and G. Volkov, arXiv:hep-ph/0008032; G. G. Volkov, Annales Fond. Broglie **31** (2006) 227 [arXiv:hep-ph/0607334].
- [20] M. Meddahi *et al.*, *In the Proceedings of Particle Accelerator Conference (PAC 07), Albuquerque, New Mexico, 25-29 Jun 2007*, pp 692.
- [21] M. Ikeda *et al.* [Super-Kamiokande Collaboration], Astrophys. J. **669** (2007) 519 [arXiv:0706.2283 [astro-ph]].
- [22] T. Totani, K. Sato, H. E. Dalhed and J. R. Wilson, Astrophys. J. **496** (1998) 216 [arXiv:astro-ph/9710203].
- [23] M. T. Keil, G. G. Raffelt and H. T. Janka, Astrophys. J. **590**, 971 (2003) [arXiv:astro-ph/0208035].
- [24] S. Hannestad and G. Raffelt, Astrophys. J. **507**, 339 (1998) [arXiv:astro-ph/9711132]; R. Buras *et al.*, Astrophys. J. **587**, 320 (2003) [arXiv:astro-ph/0205006]; M. Liebendoerfer *et al.*, Astrophys. J. **620**, 840 (2005) [arXiv:astro-ph/0310662]; G. G. Raffelt, M. T. Keil, R. Buras, H. T. Janka and M. Rampp, arXiv:astro-ph/0303226.
- [25] L. Wolfenstein, Phys. Rev. D **17**, 2369 (1978);
- [26] S. P. Mikheev and A. Y. Smirnov, Sov. J. Nucl. Phys. **42**, 913 (1985) [Yad. Fiz. **42**, 1441 (1985)]; S. P. Mikheev and A. Y. Smirnov, Nuovo Cim. C **9**, 17 (1986).
- [27] V. D. Barger, K. Whisnant, S. Pakvasa and R. J. N. Phillips, Phys. Rev. D **22**, 2718 (1980).
- [28] M. Maltoni *et al.*, New J. Phys. **6**, 122 (2004) [hep-ph/0405172]; S. Choubey, arXiv:hep-ph/0509217; S. Goswami, Int. J. Mod. Phys. A **21**, 1901 (2006); A. Bandyopadhyay *et al.*, Phys. Lett. B **608**, 115 (2005) [arXiv:hep-ph/0406328]; G. L. Fogli *et al.*, Prog. Part. Nucl. Phys. **57**, 742 (2006) [arXiv:hep-ph/0506083];
- [29] H. Duan, G. M. Fuller, J. Carlson and Y. Z. Qian, Phys. Rev. D **74** (2006) 105014 [arXiv:astro-ph/0606616]; H. Duan, G. M. Fuller, J. Carlson and Y. Z. Qian, Phys. Rev. Lett. **97** (2006) 241101 [arXiv:astro-ph/0608050]; S. Samuel, Phys. Rev. D **48** (1993) 1462; V. A. Kostelecky and S. Samuel, Phys. Rev. D **52** (1995) 621 [arXiv:hep-ph/9506262]; J. T. Pantaleone, Phys. Rev. D **58** (1998) 073002; S. Samuel,

- Phys. Rev. D **53** (1996) 5382 [arXiv:hep-ph/9604341]; G. G. Raffelt and A. Y. Smirnov, Phys. Rev. D **76** (2007) 081301 [Erratum-ibid. D **77** (2008) 029903] [arXiv:0705.1830 [hep-ph]]; G. G. Raffelt and A. Y. Smirnov, Phys. Rev. D **76** (2007) 125008 [arXiv:0709.4641 [hep-ph]]; B. Dasgupta and A. Dighe, arXiv:0712.3798 [hep-ph].
- [30] R. Tomas, M. Kachelriess, G. Raffelt, A. Dighe, H. T. Janka and L. Scheck, JCAP **0409**, 015 (2004).
- [31] T. J. Loredo and D. Q. Lamb, Phys. Rev. D **65** (2002) 063002 [arXiv:astro-ph/0107260].
- [32] R. Tomas, D. Semikoz, G. G. Raffelt, M. Kachelriess and A. S. Dighe, Phys. Rev. D **68** (2003) 093013 [arXiv:hep-ph/0307050].
- [33] A. Bueno, I. Gil-Botella and A. Rubbia, arXiv:hep-ph/0307222; I. Gil-Botella and A. Rubbia, JCAP **0310** (2003) 009 [arXiv:hep-ph/0307244]; I. Gil-Botella and A. Rubbia, JCAP **0408** (2004) 001 [arXiv:hep-ph/0404151].
- [34] See, e.g., <http://ieee1588.nist.gov/>.
- [35] M. A. Lombardi, L. M. Nelson, A. N. Novick and V. S. Zhang, *Time and Frequency Measurements Using the Global Positioning System*, Cal. Lab. Int. J. Metrology, (July-September, 2001) 26-33; see also: <http://tf.nist.gov/time/oneway.htm>; <http://tf.nist.gov/time/commonviewgps.htm>.
- [36] M. A. Lombardi and A. N. Novick, *Comparison of the one-way and common view GPS measurement technique using a known frequency offset*, Proceedings of 34th Annual Precise Time and Time Interval (PTTI) Meeting; see also: <http://tycho.usno.navy.mil/ptti/ptti2002/paper4.pdf>.
- [37] K. Larson and J. Levine, *Carrier-Phase Time Transfer*, IEEE Trans. On Ultrasonics, Ferroelectrics and Frequency Control, **46**, (1999) 1001; see also: <http://tycho.usno.navy.mil/gpscp.html>.
- [38] See, for example: D.L. Band, Ap. J. **486**, (1997) 928; J. P. Norris, G. E. Marani and J. T. Bonnell, Ap. J. **534**, (2000) 340.